8-2024

Dynamic Modeling of a Nuclear Integrated Energy System With Thermal Energy Storage and Hydrogen Production

Seth J. Dana
Utah State University

DYNAMIC MODELING OF A NUCLEAR INTEGRATED ENERGY SYSTEM WITH THERMAL ENERGY STORAGE AND HYDROGEN PRODUCTION

by

Seth J. Dana

A thesis submitted in partial fulfillment
of the requirements for the degree

of

MASTER OF SCIENCE

in

Mechanical Engineering

Approved:

Hailei Wang, Ph.D. Major Professor	Nick Roberts, Ph.D. Committee Member
Tiyani He, Ph.D. Committee Member	D. Richard Cutler, Ph.D. Vice Provost for Graduate Studies

UTAH STATE UNIVERSITY
Logan, Utah

2024

ABSTRACT

Dynamic Modeling of a Nuclear Integrated Energy System with Thermal Energy Storage and Hydrogen Production

by

Seth J. Dana, Master of Science

Utah State University, 2024

Major Professor: Hailei Wang, Ph.D.
Department: Mechanical and Aerospace Engineering

Advanced nuclear reactors, such as the Natrium design by TerraPower and GE Hitachi, operate at higher temperatures, making them suitable for co-located hydrogen production. This paper models and analyzes three Natrium systems with thermal energy storage and co-located hydrogen production using high temperature electrolysis. The first two configurations focus on improving thermal efficiency of the Rankine cycle, while the final configuration improves hydrogen production efficiency. A techno-economic analysis determines the economic benefit of hydrogen production and storage for three energy markets in the United States: California, Texas, and the Midwest region. California and Texas are considered volatile energy markets while the Midwest market is less volatile. These results are compared to the baseline Natrium system with no hydrogen production. Results indicate that coupling the Natrium system with hydrogen production can boost Rankine cycle efficiency by 1%, and using low grade steam from the Natrium steam cycle as feedstock for hydrogen production increases the overall system efficiency by 3%. The techno-economic analysis demonstrates that integrating the Natrium system with hydrogen production enhances the economic viability, particularly in regions with less volatile and lower electricity prices. Incorporating hydrogen storage into the system enhances plant flexibly, which is

advantageous in volatile electricity markets. In addition, hydrogen production and storage offer economic stability in markets with volatile electricity prices due to its constant price and production rate.

(102 pages)

PUBLIC ABSTRACT

Dynamic Modeling of a Nuclear Integrated Energy System with Thermal Energy Storage and Hydrogen Production

Seth J. Dana

Historically, nuclear reactors have used water for cooling and moderating the nuclear reaction within the core. Advanced generation IV nuclear reactors currently under development are designed with different coolants which enable operation at higher temperatures. A higher operating temperature makes nuclear power suitable for co-located hydrogen production via high temperature electrolysis. Natrium, an advanced reactor design by TerraPower and GE Hitachi, combines a sodium fast reactor with molten salt thermal energy storage. The work presented in this thesis models and analyzes three Natrium systems which integrate hydrogen production with the Natrium nuclear power plant. The first two configurations focus on improving thermal efficiency of the electricity generation while the third and final configuration improves hydrogen production efficiency. A techno-economic analysis of the Natrium system with co-located hydrogen production in three US locations (California, Texas, and Midwest states) determines the economic benefits of hydrogen production and storage coupled with the Natrium design. Results indicate that coupling the Natrium system with hydrogen production can boost thermal efficiency of the Natrium steam cycle by 1%, and using steam from the steam cycle as feedstock for hydrogen production increases overall system efficiency by 3%. The economic analysis demonstrates that integrating the Natrium system with hydrogen production enhances the economic viability, particularly in regions with less volatile and lower electricity prices. Incorporating hydrogen storage into the system enhances plant flexibly, which is advantageous in volatile electricity markets. In addition, hydrogen production and storage offer economic stability in markets with volatile electricity prices due to its constant price and production rate.

ACKNOWLEDGMENTS

I would like to recognize and express my gratitude to my advisor Dr. Hailei Wang who has mentored and taught me since my undergraduate studies at Utah State University. He introduced me into the nuclear and hybrid energy systems area of research and made my time at Utah State a positive and impactful experience.

Besides my advisor, I would also like to thank Aiden Meek for his knowledge and assistance with system modeling, Jacob Bryan for his expertise in energy systems, synthetic time series, and INL's RAVEN framework, and Manjur Basnet for his assistance in training synthetic time histories. Their help and collaboration was monumental in the completion of this work.

Most importantly, I want to thank my beautiful wife Maddie Dana. You have been by my side throughout this entire journey and your support gave me the courage, commitment and belief in myself to complete this work. I want you to know I recognize all of the support and patience you have shown me and I'm so excited for our future and what good things it holds for us. I love you!

Finally, I would like to express my gratitude to the Nuclear Energy University Program (NEUP) and the Nuclear Regulatory Commission (NRC) for funding this research and enabling me to further my education. Additionally, I would like to acknowledge the Nuclear Energy Agency (NEA) Nuclear Education, Skills, and Technology (NEST) fellowship for offering valuable workshops and international conference experiences in the nuclear industry.

Seth J. Dana

CONTENTS

LIST OF TABLES

LIST OF FIGURES

CHAPTER 1

INTRODUCTION

1.1 Motivation of Research

According to the US energy information agency, residential consumption of purchased electricity in the United States is projected to increase between 14% - 22% by 2050 [1]. Industrial energy consumption could increase by as much as 32% in that same time frame [1]. Furthermore, in 2022 electric vehicles (EVs) made up 7% of US vehicle market, as the adoption of electric vehicles is projected to increase, the electricity purchase for EVs is projected to increase by 900% - 2000% up to 381 TWh (1.3 quads) in 2050 [1]. In addition to the increasing demand of electricity, the US government has goals for the power sector to be carbon free by 2035. This ambitious goal will require a wave of new carbon free utilities such as nuclear, solar, and wind power to be added to the grid. This goal also entails removing/repurposing significant power production facilities that use coal or natural gas. Coal and natural gas accounted for 60.2% of electricity generation in the US during 2022 [2].

In addition to the need for carbon free electricity, many industrial processes contribute to the large amounts of greenhouse gasses being released into the environment, including, hydrogen production. Hydrogen is used as rocket fuel, to power vehicles, refining, and ammonia production. Currently in the US, 95% of hydrogen is produced with natural gas through a process called steam-methane reformation [3]. This requires high temperature steam (700-1000 °C) and natural gas (CH4) which is reacted together to produce hydrogen, carbon monoxide (CO), and carbon dioxide (CO2). Hydrogen can also be produced without the use of fossil fuels using a process called high temperature electrolysis (HTE). HTE is a method that separates high temperature steam into hydrogen and oxygen using electricity. Currently, it is not economically advantageous to use this method due to the low cost of hydrocarbons. However, if this technology were to be coupled with nuclear power it could

become economically viable. Nuclear power has the ability to provide both high temperature steam and electricity required to produce green hydrogen using HTE.

Advancing nuclear technology, energy storage, and the need for carbon free hydrogen have paved the way for the capability of co-located nuclear plants and HTE facilities. This would provide a future solution to creating carbon free electricity and hydrogen. Hydrogen production on site would also provide long term energy storage for nuclear power plants. Electricity demand trends in the US follow daily and seasonal patterns. The demand in the hot summer months can significantly increase compared to the winter. Seasonal hydrogen storage could be used as a way to reach summer peaks without the need for plants with larger capacity.

Hydrogen storage methods can be placed in two categories: physical-based or material based [4]. Physical-based storage stores the hydrogen as a compressed gas or, in some cases, as a liquid at cryogenic temperatures. The most common method is compressed gas storage. In energy storage applications, hydrogen is compressed and stored in tanks or salt caves at up to 170 bar. Material-based storage involves storing hydrogen in materials such as metal hydrides or nanomaterials with porous molecular structures to allow the storage of gaseous hydrogen. There are many technological challenges with material-based storage methods as of now. Compressed gas storage is the current economic choice for hydrogen storage. With hydrogen production and storage closely coupled with the nuclear power plant there are opportunities for waste heat recovery which will increase cycle efficiency and increase the economic outcome of the nuclear reactor.

The Natrium design includes a sodium fast reactor coupled with a two-tank molten salt thermal energy storage (TES) system, which can provide energy during periods of high demand or when renewable energy sources are not available. It is designed to physically separate the energy storage and conversion systems (the Energy Island) from the reactor system (the Nuclear Island). This separation of nuclear island and energy island make the Natrium design very suitable for various NHES configurations. Electricity production can be coupled with hydrogen production, clean water production, and electricity generation,

while integrating with local renewables. This work aims to design and model a Natrium based NHES with co-located hydrogen production through HTE using Modelica. This work will investigate how co-locating these two processes benefit the economics of nuclear power, how waste heat recovery from hydrogen storage can benefit electricity generation, and how hydrogen and energy markets affect optimal plant operation. Figure 1.1 shows a potential NHES configuration coupled with renewable energy and hydrogen production.

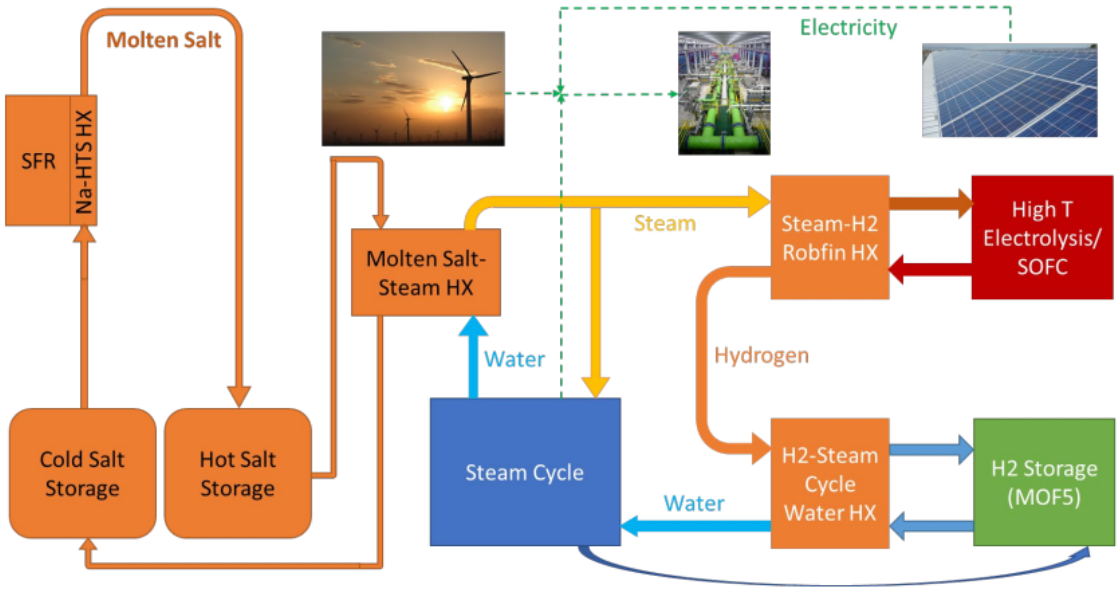

Fig. 1.1: Schematic of Natrium NHES design concept couples with hydrogen production and storage.

1.2 Literature Review

Climate change as a result of greenhouse gas emissions is a threat to out planet and its inhabitants. The consequences of global warming, including rising sea levels [5], extreme weather events [6], and food and water scarcity [7], are already being felt worldwide. Human activities are the primary source of the increase of greenhouse gases in the atmosphere over the last 150 years [8]. To mitigate these impacts, many countries are beginning a transition away from fossil fuels towards carbon free technologies to generate electricity without emitting greenhouse gases [9]. Transportation, electric power generation, and industrial processes combine to contribute 76% of greenhouse gas emission in the US [8]. The transportation sector is already beginning to electrify which will put a greater strain on power generation in the coming years [10].

Renewable energy technologies like photovoltaic (PV) solar panels, wind turbines, and concentrated solar power (CSP) have been introduced into the scene to provide renewable, carbon free electricity. Deployment of solar panels surged from 0.26 GW in 2000 to 16.1 GW in 2010, according to a study by Branker et al. [11]. Figure 1.2 from the Lawrence Livermore National Laboratory shows the energy consumption of the US in 2021 by source [12]. It clearly shows that coal and natural gas supply the nation with the majority of its power, while renewables only scratch the surface.

In some energy markets around the United States, the installment of renewable technologies, such as wind and solar, have created an more volatile energy demand for traditional power plants to meet. This is due to varying and unpredictable weather conditions that renewable systems rely on. Historically, nuclear power plants have primarily been used for base load electricity generation, and their operation may not be well-suited for fluctuating loads. While the technology and capability for load following nuclear power plants is available, the limiting factor preventing nuclear plants from load following comes from the economics due to a reduction in capacity factor [13]. The majority of the cost of a nuclear power plant is the upfront capital cost while the operating and fuel costs are relatively low compared to their capital expense [14]. This 'front-loaded' cost structure and low fuel cost

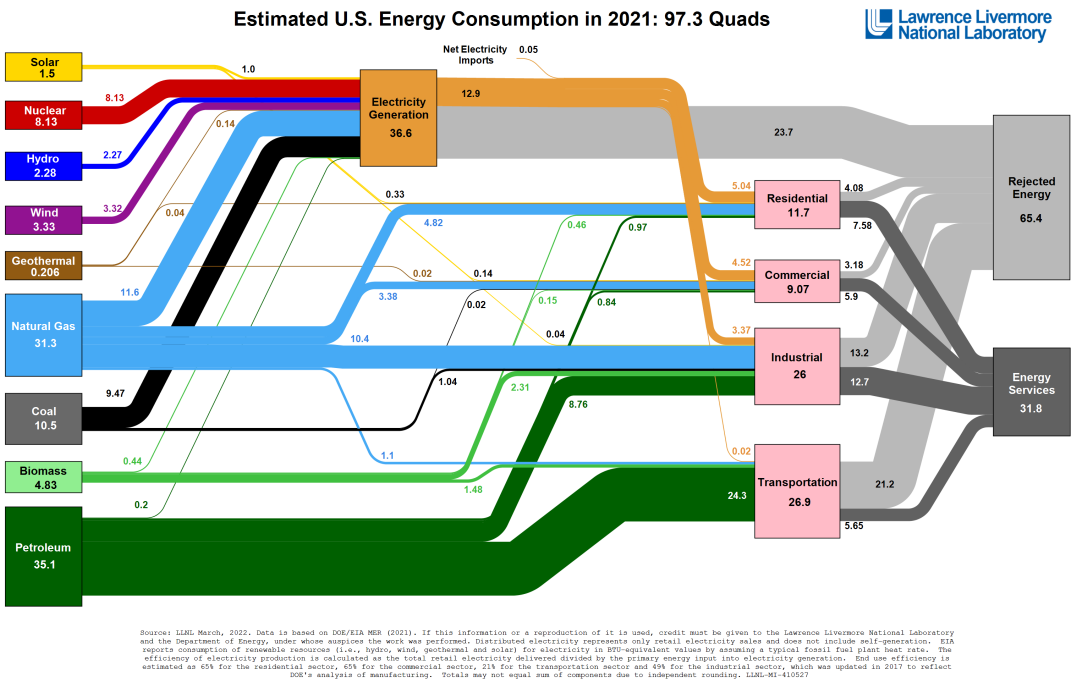

Source: LLNL March, 2022. Data is based on DOE/EIA MER (2021). If this information or a reproduction of it is used, credit must be given to the Lawrence Livermore National Laboratory and the Department of Energy, under whose auspices the work was performed. Distributed electricity represents only retail electricity sales and does not include self-generation. EIA reports consumption of renewable resources (i.e., hydro, wind, geothermal and solar) for electricity in BTU-equivalent values by assuming a typical fossil fuel plant heat rate. The efficiency of electricity production is calculated as the total retail electricity delivered divided by the primary energy input into electricity generation. End use efficiency is estimated as 65% for the residential sector, 65% for the commercial sector, 21% for the transportation sector and 49% for the industrial sector, which was updated in 2017 to reflect DOE's analysis of manufacturing. Totals may not equal sum of components due to independent rounding. LLNL-MI-410527

Fig. 1.2: Estimated U.S. energy consumption in 2021 by source. Electricity generation sources natural gas and coal account for 58% consumed [12].

(10% - 15% of electricity generation cost [15]) make constant base load power scenarios attractive for nuclear power [14]. In the case of fossil fuels, the operating costs dominate. Fuel costs account for 70% - 80% of the electricity generation cost [15].

Electric load following with the reactor alone requires modifying reactivity in the core by moving control rods in/out of the core. Reducing reactivity in the core wastes potential energy of the fuel and can cause thermal strain on the nuclear system [16]. Co-generation and thermal energy storage (TES) are two ways for nuclear power to load follow without the need to modify reactivity in the core [17]. Co-generation involves the production of electricity and another valuable product using energy from a single nuclear source. This other valuable product can be clean water through desalination, hydrogen production, or energy storage [18]. When the demand for electricity is high the plant will produce more electricity and when it is low the secondary product will be produced. This allows a nuclear plant to match with a variable electricity load while operating at a steady state on the

nuclear side. The focus of this thesis will be nuclear power generation with hydrogen co-generation which will increase plant flexibility and may increase economic viability for nuclear power. These systems with multiple energy sources and products are often called integrated energy systems (IES) or nuclear hybrid energy systems (NHES). Nuclear is a clear candidate for IES due to its ability to reliably produce large amounts of electricity and heat with a low carbon footprint.

Many researchers have investigated different nuclear IES. Hill et al. [19] studied a small modular reactor (SMR) IES coupled with freeze and reverse osmosis desalination techniques. Freezing water as a method of desalination provides cold thermal energy storage that could be utilized in the condenser to boost power production and efficiency during peak hours. Bryan et al. [20] studied the deployment of a Natrium style nuclear IES with two tank molten salt energy storage and hydrogen production with salt cavity storage in Texas. They concluded that the system could produce large amounts of hydrogen during off peak times, mainly in the spring and fall. They also concluded that the hydrogen fuel cell used to meet peak demands in the summer had a capacity factor of 3.1% and did not meet the economic goals of the study. Frick et al. [21] from Idaho National Lab investigated retrofitting existing pressurized water reactors for hydrogen co-generation. They developed a comprehensive cost estimation and analyzed electricity and hydrogen markets in the Pennsylvania-New Jersey-Maryland (PJM) interconnect. Utilizing these models, they concluded that positive motivations can be found for hydrogen co-generation at all hydrogen market pricing projections. Wodrich et al. [22] developed a model in Modelica language to investigate deployment scenarios for micro-reactors in an energy diverse grid on a university campus. They concluded that using a micro-reactor solely to produce electricity would have the greatest impact on emission reduction. While dynamic operation using molten salt energy storage benefited by having a lower dependence on grid connection but showed lower emissions reduction and cost savings. Binder et al. [23] modeled a nuclear, wind, and chemical plant hybrid energy systems (HES). They concluded that Modelica could be effec-

tively used to model large complex systems with dynamic conditions and added significant advantage to evaluating control algorithms.

1.3 High Temperature Steam Electrolysis

Producing hydrogen without emitting greenhouse gasses will be essential for the hydrogen market in the near future. Current practices of using steam methane reforming to produce hydrogen will not be able to continue as the push for eliminating carbon emissions intensifies. Hydrogen can be produced without emitting carbon emissions through electrolysis. Conventional alkaline water electrolysis is a proven technology, however, this process requires large amounts of electricity which results in a poor efficiency and high operating cost [24]. Electricity cost can account for 80% of the total selling price of hydrogen using alkaline water electrolysis on a large scale [25].

High temperature steam electrolysis can increase the efficiency of the electrolysis process and reduce electricity requirements. High temperature steam electrolysis requires steam temperatures of 800+ °C. When coupled with advanced reactor technologies, the heat and electricity required can be provided. Advanced reactors such as liquid sodium and high temperature gas cooled reactors are being considered for hydrogen production due to their high outlet temperature conditions. The total energy required for steam electrolysis, ΔH is

$$\Delta H = \Delta G + Q_{es} \tag{1.1}$$

where ΔG is the gibbs free energy change and Q_{es} is the thermal energy demand for the electrolysis [26]. The electricity that will be used in the HTE will come from the nuclear reactor so it can be determined by

$$\Delta G = \eta_{th} Q_{N,el} \tag{1.2}$$

with η_{th} being the thermal efficiency of the nuclear power cycle (Rankine cycle) and $Q_{N,el}$ is the thermal energy from the nuclear reactor used to produce electricity. The total thermal

energy required for the high temperature steam electrolysis (Q_{es}) is the sum of heat required from the nuclear reactor to produce the electricity for electrolysis and to heat steam and sweep gasses up to ∼850°C.

$$Q_{es} = Q_{N,el} + Q_{N,es} \tag{1.3}$$

Gibbs free energy, thermal energy required, and the total energy required for electrolysis change with temperature. Figure 1.3 shows how these variables change with temperature. As the temperature of steam electrolysis increases, ΔH also increases while ΔG decreases due to an increase of Q_{es}.

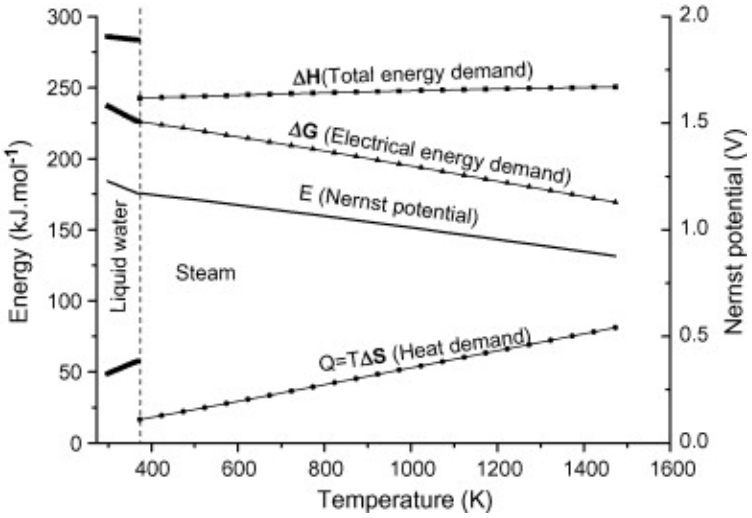

Fig. 1.3: Energy demand for steam electrolysis vs temperature [27].

The ratio of ΔG to ΔH at 100 °C is 93% and is reduced to 70% at 1000 °C. This means that higher temperature electrolysis requires less electrical power which increases thermal to hydrogen energy conversion efficiency [27]. Another benefit of high temperature electrolysis is that it increases electrode activity in the stack and lessens cathodic and anodic

overpotential which is when the actual cell voltage required for a reaction is higher than the theoretical value.

1.4 Hydrogen Storage

A nuclear power plant co-located with hydrogen production and storage would provide clean electricity and hydrogen. Having the hydrogen production and storage closely coupled with the nuclear plant creates opportunities for increased thermal efficiency, enhanced flexibility, and better economic performance of the nuclear system.

The concept in Fig. 1.1 is a configuration of a nuclear IES coupled with hydrogen production. The hydrogen is produced using HTE and stored in metal-organic frameworks (MOFs). MOFs are metal ions arranged with organic linkers in a porous dimensional structure. These physical characteristics and tunability make gaseous hydrogen storage possible. MOF-5 is the prominent design made up of Zn_4O cluster and 1,4-benzo dicarboxylic acid as the organic linker [28]. MOFs are still being investigated and studied for hydrogen storage applications.

Another method of hydrogen storage that can be coupled with a nuclear-hydrogen IES is compressed gas storage in natural (or artificial) salt caverns. This method of gaseous storage is already being used with natural gas. Figure 1.4 shows a schematic view of natural gas storage in a salt cavern [29]. Using a similar method for hydrogen provides opportunities to recover significant amounts of energy during the compression of hydrogen.

Today there are three sites that use underground salt caves to store hydrogen. Clemens USA, Moss Bluff USA, and Teesside UK [30] with many more locations used for natural gas [29]. Table 1.1 highlights the details of these hydrogen storage systems. The operation of these hydrogen storage sites have demonstrated the reliability of this technology. Salt caverns can be 10 times less expensive than above ground tank storage and 20 times less expensive as hard rock mine storage, thus giving salt caverns an economic edge [31]. Salt cavity hydrogen storage is advantageous to other forms of storage due to its ability to quickly change from storage/discharge states, even at high pressure [32]. These facilities can also perform many cycles during the year where traditional, seasonal gas storage only performs a

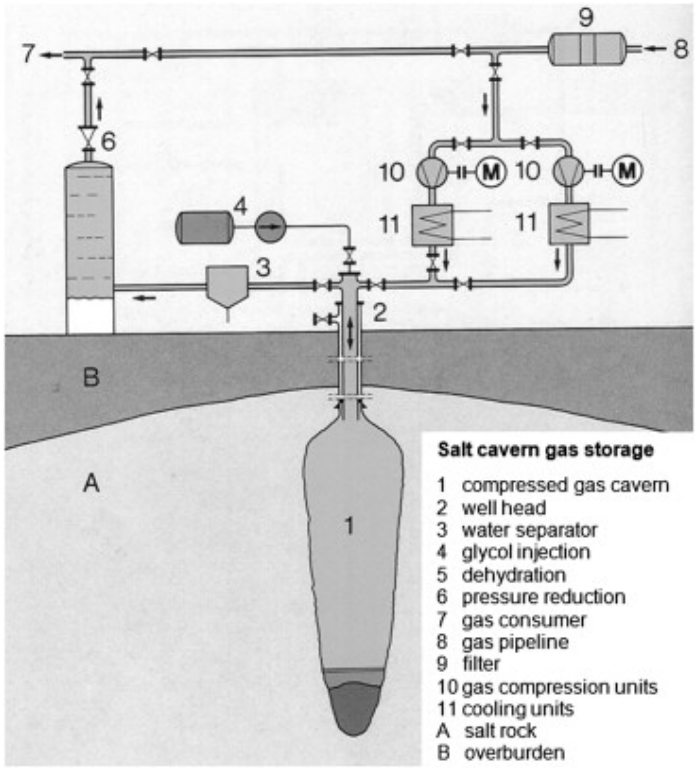

Fig. 1.4: Schematic of natural gas storage in salt cavern.

single seasonal cycle per year [32]. A disadvantage to salt cavity storage is the construction period can be very long (years) for artificial construction of salt cavities. However, the reduced cost and hydrogen storage potential is leading to new projects in US and Europe to build more salt cavern hydrogen storage facilities. The high construction time can be avoided if a naturally occurring aquifer or depleted natural gas/oil reserves are used for storage [33]. The Advanced Clean Energy Storage project in Delta, UT is set to combine alkaline electrolysis with two salt caverns to store clean hydrogen [34]. The electrolyzers will produce hydrogen which will be deployed as fuel in a hydrogen capable gas turbine combined cycle that will be fueled 100% by hydrogen by 2045 [35].

In literature, Wang et al. [36] investigated large scale hydrogen storage methods. They ruled out cryogenic liquid storage due to its high capital cost, and low efficiency. They concluded that above ground pressure vessels can be economic for large scale storage. However,

Table 1.1: Details of existing salt cave hydrogen storage cites. [30]

	Clemens (USA)	**Moss Bluff (USA)**	**Teesside (UK)**
Geology	Domal Salt	Domal Salt	Bedded Salt
Operator	Conoco Phillips	Praxiar	Sabic Petroleum
Stored Fluid	Hydrogen	Hydrogen	Hydrogen
Commissioned	1983	2007	∼1972
Volume [m^3]	580,000	566,000	3 x 70,000
Reference depth [m]	930	>822	350
Pressure range [bar]	70 - 135	55 - 152	∼45
Possible working gas capacity H_2 [kg]	2.56e6	3.72e6	0.83e6

if the system needs flexible operation capabilities due to unpredictable renewable energy availability, then salt cavity storage is more suitable due to its larger capacity. Ma et al. [37] highlighted some of the challenges associated with production of green hydrogen, such as, hydrogen transportation and storage. They concluded that compressed hydrogen storage in geological repositories is a promising method, however, can experience energy losses which lowers overall efficiency. Introducing hydrogen into existing natural gas pipelines showed potential for transporting hydrogen but is limited by capabilities of appliances and equipment designed specifically for natural gas. They expect the cost of storing and transporting green hydrogen to decrease in the future due to technology advancement and economy of scale. Tarhan et al. [38] summarized hydrogen storage methods and claim that the future of industrial hydrogen storage is solid state storage methods. This included complex hydrides, chemical hydrides, magnesium-based alloys, and intermetallic compounds. These methods have large potential for storing hydrogen at low pressures, however, have challenges surrounding cost, hydrogen extraction, limited lifespan, and transportation safety.

1.5 Nuclear Hydrogen IES Modeling

A dynamic model of a nuclear IES with co-located hydrogen production will provide insight to how these two systems will integrate and operate. The molten salt energy storage system in the Natrium design allows the reactor to operate at a a fixed heat output, while electricity production can vary according to the changing energy demand. This flexibility is essential in managing the volatility of renewable energy sources and meeting the varying energy demands of different regions. A Natrium system coupled with hydrogen production can give the energy island even more flexibility while also providing a potential boost to thermal efficiency. The Natrium reactor is a sodium fast reactor, as such the coolant temperature is greater than a typical Gen III light water or boiling water reactor. The steam temperature the Natrium reactor can provide for HTE is greater which is expected to reduce the topping heat required in the HTE process.

Systems with compressed gas storage will require the hydrogen to be compressed to the required pressure depending on storage method and capacity. Compressing hydrogen will increase the temperature which can be used to preheat feedwater in the Rankine cycle. Hydrogen is an excellent energy carrier with a large heat capacity. At 300 K the specific heat of hydrogen, c_p, is 3.4 times larger than water. This mean high temperature hydrogen is carrying a significant amount of energy that can be recovered. Hydrogen exiting the HTE process will also require significant cooling before being compressed for storage. This provides another opportunity for heat recovery that can be used in the balance of plant.

CHAPTER 2

OBJECTIVES

1. Develop dynamic Modelica models of Natrium IES with co-located hydrogen production and storage.

2. Investigate IES configurations between the Natrium and HTE systems, and quantify the improvement on the thermal efficiency of the Natrium power cycle.

3. Investigate hydrogen storage in salt cavities and how to thermally integrate it with Natrium and HTE systems.

4. Perform case studies of the optimal Natrium IES with and without salt cavity hydrogen storage, and evaluate their NPV compared to the Natrium baseline design for power generation only using INL's HERON tool.

CHAPTER 3
APPROACH

3.1 Methodology Overview

This chapter will describe the methodology and approach to accomplish the objectives listed in chapter 2.

3.2 Modelica Software

Modelica is a modern equation based object oriented modeling language for differential algebraic equation (DAE) based physical modeling. Even the most complex physical systems can be composed of elementary components. Each component can be defined by governing laws of physics. Components in Modelica are interfaced through special nodes called connectors which communicate with other components in the model [39]. This concept allows for acausal modeling in which the user does not need to define input-output relations for the variables. Commercial Modelica software environments, like Dymola [40], come with advanced compiler and implicit solvers that can manipulate and solve DAE systems allowing the modeler to focus on physical modeling rather than algorithm selection and mathematical formulation [39].

3.3 Natrium System Model and Controls

The Natrium design includes a sodium fast reactor coupled with a two tank molten salt TES system, which can provide energy during periods of high demand or when renewable energy sources are not available. The TES can additionally supply heat to a co-located industrial process, such as, hydrogen production via high temperature steam electrolysis. The Natrium system is designed to physically separate the energy storage and conversion systems (the Energy Island) from the reactor system (the Nuclear Island). The heat from the Nuclear Island is directly transferred to the TES which discharges that heat into the

energy recover system, or balance of plant (BOP), to produce electricity. Specifically, the Natrium design has a reheat Rankine cycle that converts the thermal energy from the TES into electricity.

One of the key advantages of the molten salt energy storage system is its ability to allow the Natrium reactor to operate at a fixed heat output, while the electricity production can vary according to the changing energy demand. This flexibility is essential in managing the volatility of renewable energy sources, hydrogen production, and meeting energy demands. The fluid in the molten salt energy storage tanks is molten nitrite salt (60% $NaNO_3$ and 40% KNO_3). The fluid properties of this molten salt are shown in Table 3.1. Molten nitrite salts have been used in concentrated solar power for sensible heat storage due to its thermal stability at high temperature, desireable heat transfer properties, at high temperatures up to 600°C, low vapor pressure and viscosity, non-toxicity, and non-flammability [41]. One technical complication of molten nitrite salts is their high melting temperature of 220°C which means the operating temperature inside the cold storage tank must remain above 290°C with to maintain a reasonable margin.

Table 3.1: Properties of molten nitrate salt (60% $NaNO_3$ and 40% KNO_3) [42, 43].

Property	**Solar Salt**
Melting Point ($°C$)	220
Boiling Point ($°C$)	565
Thermal Conductivity (W/mK)	0.53
Density (kg/m^3)	1804
Specific Heat Capacity (kJ/kgK)	1.52
Dynamic Viscosity ($Pa\ s$)	0.00169
Prandtl Number	4.85

The system includes a model based control scheme that follows a given demand profile, allowing the Natrium Energy Island to respond to changes in energy demand in real-time. This section will discuss major components in the Natrium system Modelica model. Figure 3.1 shows the Dymola schematic of the Natrium system.

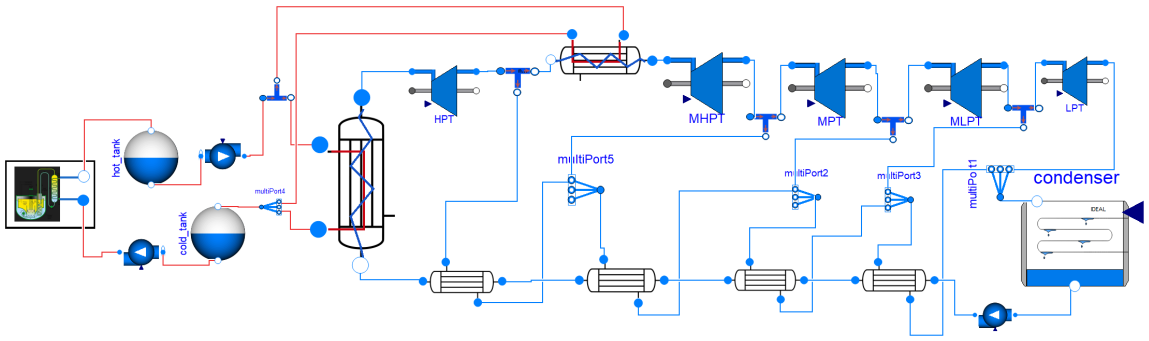

Fig. 3.1: Schematic of the Dymola model of the Natrium system.

3.3.1 System Parameters and Assumptions

This section will examine the assumptions and components that are incorporated into the model. The model does not intend to incorporate nuclear kinetics of the sodium fast reactor in the Nuclear Island; instead, it employs a simplified heat addition that simulates the constant heat input equivalent to the reactor. The molten salt will act as a coolant as it is pumped through the reactor model. The baseline electricity output of the model is set at 345 MW_e, with the capability to increase to 500 MW_e for a duration of 5.5 hours.

The system operates between power levels of 200-500 MW_e. This allows the system to store heat in the hot tank when operating below 345 MW_e. Given the system is modeled in an hour interval, the transient/dynamic behavior within an hour is not modeled. This assumes all components in the system have reasonable time constant less than 20 minutes. Thus, the system is assumed always under quasi steady state during the simulation. The steam turbines have a fixed isentropic efficiency of 87%.

3.3.2 Sodium Fast Reactor

The sodium fast reactor is modeled as a constant heat rate added to the molten salt storage. Heat is added to the molten salt storage through a volume component with a constant heat rate. The mass flow rate through the reactor is determined by,

$$Q_{in} = \dot{m}_{salt} c_{p,salt} (T_{hot} - T_{cold}) \tag{3.1}$$

where

$$Q_{in} = \frac{P_{baseload}}{\eta_{thermal}} \tag{3.2}$$

and $P_{baseload} = 345$ MW_e. The flow rate of molten salt through the reactor will remain constant during simulations. Thus, this section of the model is referred to as the Nuclear Island, while the remaining portions of the model are called Energy Island.

3.3.3 Rankine Cycle

Electricity is generated from a reheat Rankine cycle with one reheat stage and four feedwater preheaters (also called regenerators). The preheaters use steam bled from the steam turbines to heat pressurized water coming from the condenser on its way to the steam generator. Preheating the feedwater increases thermal efficiency of the steam cycle. Figure 3.3 and 3.2 show the T-s diagram and state points diagram respectively for the Rankine cycle with feedwater preheating and steam reheat after the first turbine stage.

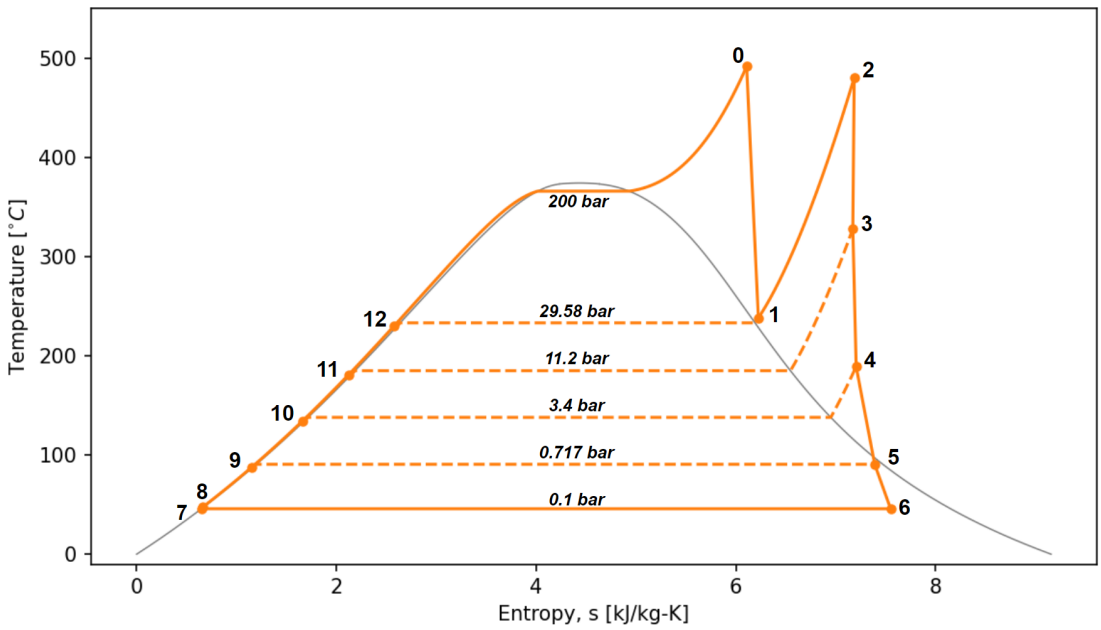

Fig. 3.2: T-s diagram of the Rankine power cycle.

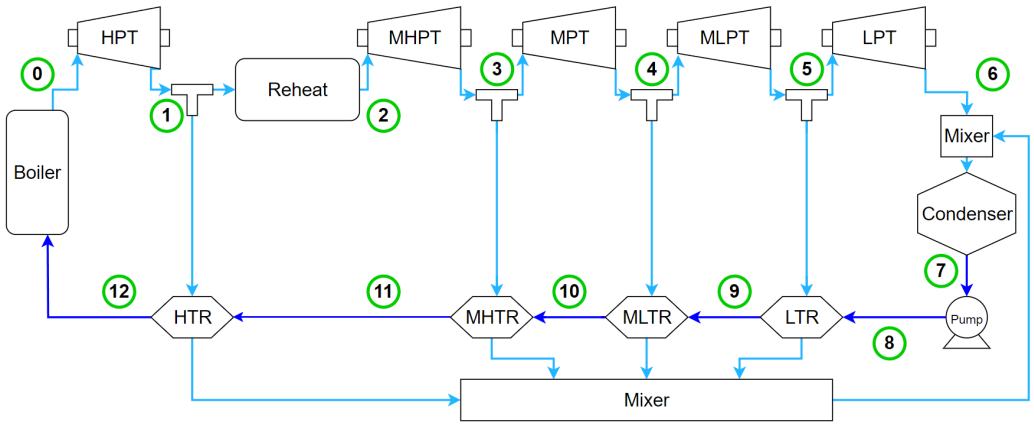

Fig. 3.3: State points of the steam cycle.

A steady state model developed in python is used to determine the optimal pressures, turbine bleed ratios, and feedwater preheat temperature stages [44]. When the turbine is operating at power levels less than the maximum (500 MW_e) the flow rate into the turbine is throttled by partial arc administration, a feature in the Modelica turbine model. The steady state python model also provides the initial pressures and temperatures at all of the state points in the dynamic model, as well as the nominal flow rates necessary for the controller. A genetic algorithm was used to determine the optimal values of the state points in the steady state model. The steady state model sets the nominal mass flow rate for power output of 500 MW_e in the dynamic Modelica model.

3.3.4 Steam Turbine

The turbine models are from the TRANSFORM Library developed by the Oakridge National Lab. They expand high pressure steam to a lower pressure to extract mechanical work due to a change in fluid volume. The following equations calculate the power produced by each turbine.

$$\dot{W} = \eta_{mech}\dot{m}(h_{in} - h_{out}) \tag{3.3}$$

In the model, the mechanical efficiency of the turbine is assumed to be 1.0, while the isentropic efficiency is equal to 0.87. The isentropic efficiency is used to calculate the outlet enthalpy of the turbine.

$$h_{in} - h_{out} = \eta_{is}(h_{in} - h_{is}) \tag{3.4}$$

The turbine is operated at power levels between 200-500 MW_e. The partial arc administration ($Arc_{partial}$) in the turbine model is used to reduce flow rate of steam into the turbine and as a result determine the outlet pressure of the turbine as shown in the following equation. The model is configured such that the partial arc admission controls the inlet of the HPT and first stage of LPT. The partial arc administration equation is given by,

$$\dot{m} = \frac{P_{out} Arc_{partial} \dot{m}_{nominal}}{P_{in,nom}} \tag{3.5}$$

The model uses 5 turbine stages to allow for steam bleeding during steam expansion to preheat the feedwater. The steam has a quality of 1.0 in all turbines except for the final stage of the LPT where the quality drops to 0.91. Thus, the Baumann factor was not considered in the turbine models.

3.3.5 Heat Exchangers

The Model contains several heat exchangers including the steam generator, reheater, and feedwater preheaters (regenerators). Most of these heat exchangers involve phase change. Boiling happens in the steam generator while condensation happens on the vapor side of the preheaters. While some of the heat exchanger models available in the open source libraries provide detailed geometry and temperature profiles they are typically computationally expensive for large system modeling, especially when the fluid experiences phase change. Since the scope of this model is a computationally inexpensive simulation without the need for exact design parameters and heat exchanger geometry, the heat exchangers in this model use an effectiveness and energy balance to determine the outlet temperatures.

The heat exchangers in the model use a modified effectiveness (ϵ) equation. Given the effectiveness, the equation can be rearranged to solve for the outlet enthalpy value,

$$h_{out,i} = h_{in,i} - \frac{\epsilon\left(\dot{m}_i \mathbf{min}(\Delta h_{max})\right)}{\dot{m}_i} \tag{3.6}$$

ϵ is the effectiveness of the heat exchanger (given), $\dot{m}_i$ is the mass flow rate, and $\mathbf{min}(\Delta h_{max})$ is the minimum of the maximum enthalpy change possible for each fluid stream,

$$\Delta h_{max} = \begin{bmatrix} \mathbf{h}(T_{1,in}, P_1, X_{1,in}) - \mathbf{h}(T_{2,in}, P_1), \\ \mathbf{h}(T_{2,in}, P_2, X_{2,in}) - \mathbf{h}(T_{1,in}, P_2) \end{bmatrix}. \tag{3.7}$$

Equations 3.6 and 3.7 are in terms of enthalpy change, instead of temperature, because of the phase change that happens in the heat exchanger. The actual heat transfer is determined by,

$$Q_{act} = \dot{m}_i \mathbf{min}(\Delta h_{max})\epsilon \tag{3.8}$$

Where $\dot{m}_i$ is the corresponding mass flow rate of the fluid stream with the minimum Δh_{max} determined in Eq. 3.7. This method does not guarantee the second law of thermodynamics is followed, however, the pinch points were checked and validated to meet the requirements of the second law. In the regenerators, in addition to ensure the second law of thermodynamics is satisfied, the outlet temperature of the feedwater is required to be 5 °C below the saturation temperature of the steam to have more reasonable regenerator size. Figure 3.4 shows how the second law of thermodynamics is satisfied in all four regenerators. As shown, there is a gap between the feedwater outlet temperature and the steam saturation temperature. After the four regenerator stages, the feedwater receives almost 350 MW as shown in the x-axis. The pinch points are also checked for the steam generator and reheater shown in the Appendix.

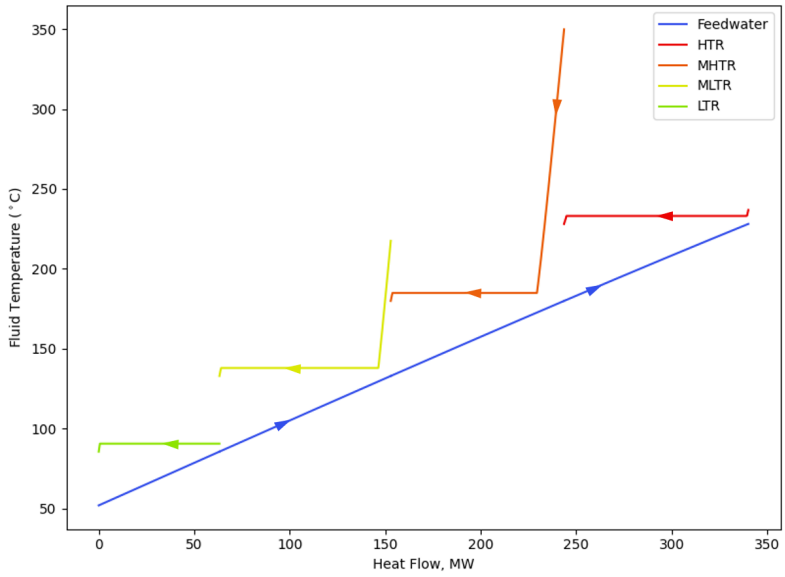

Fig. 3.4: Temperature profiles within regenerators.

3.3.6 Control Scheme

The main objective of the control system is to follow a given electricity demand profile. The control system has two actuators that change the following flow rates: 1) $\dot{m}$ from the hot tank through the steam generator to the cold tank 2) $\dot{m}$ of the Rankine cycle.

Figure 3.5 shows a simplified model diagram with labeled components, lists the controlled quantities, governed components, reference values, and operation modes. There are three modes of operation:

1. Charging: When the demand is less than 345 MW_e
2. Boosting: When the demand is greater than 345 MW_e
3. Steady State: When the TES is full/empty the system goes to steady state operation at 345 MW_e

The electrical output of the system is controlled by the mass flow rate in the feedwater pump. The python steady state model calculated the nominal flow rate for the steam cycle

at maximum power. However, the efficiency of the turbines and complexity of integrating the Natrium power cycle with hydrogen production will make the relationship between mass flow rate of steam and power output change with system conditions. A PI controller from the TRANSFORM library is utilized to control the power output of the Natrium steam cycle. The PI controller measures the current power output and compares it to the desired power output and outputs a value between 0 and 1. This value is multiplied by the nominal flow rate which will control the system to produce the desired amount of electricity.

The steam pressure in the high pressure turbine (HPT) is controlled using partial arc admission. This is similar to throttling, however, it does not consider thermodynamic losses [45]. Steam temperature at the outlet of the steam generator is controlled by the mass flow rate of molten salt in the steam generator. During steady state operation, the level in both the hot and cold tank must remain constant. The mass flow rate of the hot tank pump (HTP) is set equal to the mass flow rate of the cold tank pump (CTP). This keeps the level in each tank constant. To maintain the state points in the steam cycle during steady state operation, power is generated at the nominal level 345 MW. The salt temperature in the hot tank is controlled by the mass flow rate of cold salt through the sodium fast reactor. The feedwater control valve (FTV) control how much steam is bled from the turbines for preheating. A PI controller which measures the final temperature of the feedwater before the steam generator inlet will control how much steam to bleed.

Table 3.2: List of controlled quantities, governed components, reference values, and operation modes for controls.

Controlled Quantity	**Governed Component**	**Reference Value**
Electrical Output	Feedwater Pump	Demand
Steam Pressure HPT	HPT Partial Arc Admission	200 bar
Steam Temperature	HTP	490°C
Steam Reheat Temp.	HTP	480°C
Salt Temp. Hot Tank	CTP	520°C
Feedwater Preheat Temp.	FTV	230°C

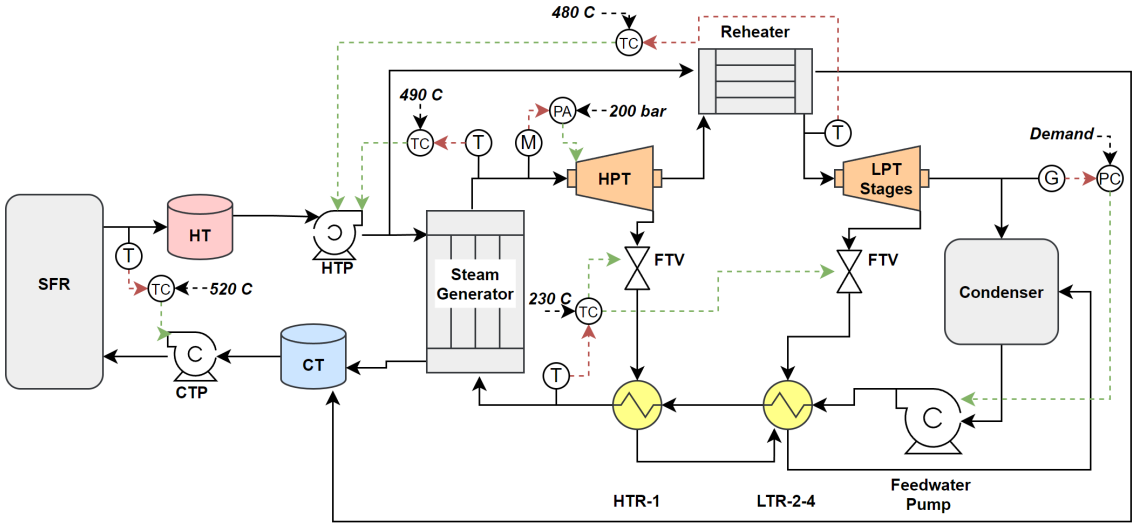

Fig. 3.5: Simplified model diagram with control signals. Sodium fast reactor (SFR), hot tank (HT), hot tank pump (HTP), cold tank pump (CTP), cold tank (CT), high pressure turbine (HPT), low pressure turbine (LPT) stages, high temperature regenerator (HTR), low temperature regenerator (LTR), feedwater temperature valve (FTV). Three LPT stages and two feedwater regenerators are not shown in this diagram.

3.4 High Temperature Steam Electrolysis Model

Idaho national laboratory has developed a high temperature electrolysis model that will be leveraged and modified for this project [46]. While the original model was designed for steam generation in connection with a NuScale SMR module, its adaptation for the Natrium system involves leveraging molten salt as a heat source. In the proposed design, molten salt from the hot tank will be utilized to produce steam within the HTE model. Once the HTE model is integrated with the Natrium model, the size of the HTE will be scaled up to 800 MW_{th}. Figure 3.6 shows the design of the HTE model. Inside the HTE vessel there are topping heaters for both the cathode (steam) and anode (air) to achieve the required state points for the electrolysis shown in Fig. 3.7. Table 3.3 shows the inputs and outputs of the HTE model at the nominal design size for the NuScale SMR. Multi-stage compression system (MSCS), feedwater pump (FWP), electric topping heater (ETH), and the electrolyzer all consume power to operate the HTE. Hot oxygenated gas leaving

the HTE vessel is used to generate a small amount of electricity in the sweep-gas turbine (SGT).

Table 3.3: Hydrogen production summary of the HTE model at baseline capacity [46]. [a]The thermal equivalent of the electrical power with a thermal efficiency of 40.0%. [b]The rate of heat flow expressed in terms of the electrical power output equivalent with thermal efficiency of 40.0%.

	Description		**Unit**	**Value**
Inputs	Water		kg/s	4.48
	Air		kg/s	23.3
Outputs	Hydrogen		kg/s	0.4015
	(Oxygen)		kg/s	3.186
	CO_2		kg/s	0
Summary	Power consumption	Total	MW_e [MW_{th}]	61.2 [153[a]]
		Electrolyzer	MW_e [MW_{th}]	45.5 [113.75[a]]
		MSCS	MW_e [MW_{th}]	10.1 [25.25[a]]
		FWP	MW_e [MW_{th}]	0.0127 [0.03175[a]]
		ETHs	MW_e [MW_{th}]	5.61 [14.0[a]]
	Power generation	SGT	MW_e [MW_{th}]	7.89 [19.7[a]]
	Nuclear process heat		MW_{th} [MW_e]	14.6 [5.84[b]]

Integrated with a small modular light-water reactor, the hydrogen product exits the HTE model at 345 °C and 17.3 bar. At this point the hydrogen product is a mixture of steam and hydrogen. This mixture is cooled until the steam condenses which allows the hydrogen and water to be separated. This hydrogen product has a significant amount of heat that can be recovered.

In the context of the Natrium system, its sodium fast reactor operates at elevated temperatures, the hydrogen product leaving the HTE is notably hotter than the nominal HTE model. Specifically, it exits at 494 °C and 17.3 bar. The higher temperature of the hydrogen product aligns with the elevated operational conditions of the Natrium system. The following section will discuss various methods to effectively recover and utilize the excess heat remained in the hydrogen product. It is anticipated that the heat recovered from the

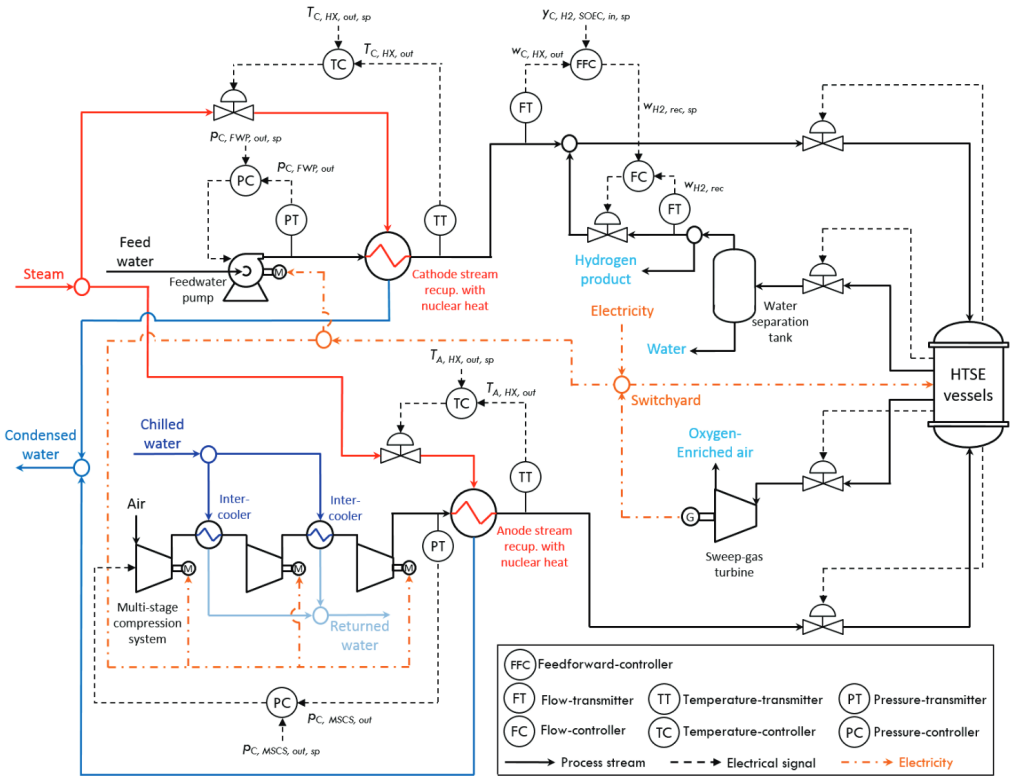

Fig. 3.6: Process flow design for the HTE [46].

hydrogen product will notably increase the thermal efficiency of the Natrium power cycle, illustrating the benefits of integrating advanced technologies for sustainable and enhanced energy conversion.

3.5 Natrium IES Coupled with Hydrogen Production

This section will discuss different innovative configurations of the Natrium IES with hydrogen production. Instead of using steam from the light-water reactor to provide the latent heat needed for the HTE, molten salt provides the thermal energy needed to vaporize the water entering the HTE for all configurations below. First, the baseline Natrium system will be described which does not include any thermal coupling of the hydrogen production. Then, three different configurations with various complexity will be discussed which include thermal coupling of the hydrogen production.

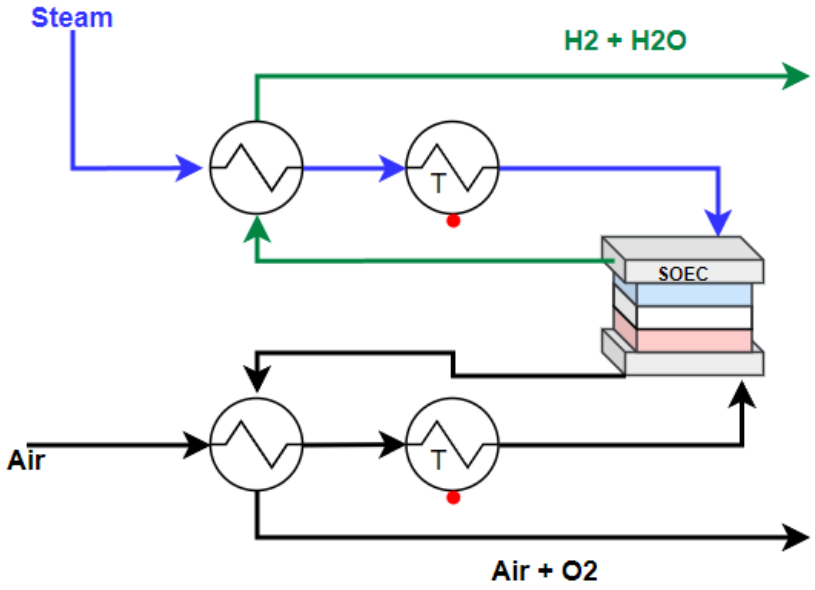

Fig. 3.7: Diagram of recuperators, topping heaters, and solid oxide electrolyzer cell (SOEC) inside the HTE vessel.

Figure 3.8 shows the baseline Natrium system with high temperature steam electrolysis. In the baseline configuration, molten salt is used to vaporize the cathode (water) sources, while the anode (air) source is preheated with the sweep gasses leaving the stack. The molten salt operates from temperatures 520 °C to 310 °C. This heats the cathode stream to the HTE vessel more than the nominal HTE model described earlier. This higher temperature increases the temperature of the hydrogen product and reduces the power consumption of the electrical topping heaters inside the vessel. The nominal HTE model consumes 5.61 MW for the electrical topping heaters while the baseline Natrium HTE model consumes 5 MW. Table 3.4 shows the utility summary of the baseline model of Natrium coupled with HTE. The mass flow rates of produced hydrogen and oxygen, as well as the input cathode and anode streams, match those of the nominal HTE model integrated with the NuScale SMR (shown in Table 3.3)

Notable differences in the utility summary of the baseline Natrium with HTE compared to the NuScale with HTE include the electrical topping heater power consumption, sweep

Table 3.4: Natrium coupled with HTE baseline utility summary. [a]The thermal equivalent of the electrical power with a thermal efficiency of 40.0%. [b]The rate of heat flow expressed in terms of the electrical power output equivalent with thermal efficiency of 40.0%.

	Description		**Unit**	**Value**
Utility	Power consumption	Total	MW_e [MW_{th}]	60.54 [151.35[a]]
		Electrolyzer	MW_e [MW_{th}]	45.5 [113.75[a]]
		MSCS	MW_e [MW_{th}]	10.03 [25.08[a]]
		FWP	MW_e [MW_{th}]	0.0127 [0.03175[a]]
		ETHs	MW_e [MW_{th}]	5.00 [12.5[a]]
	Power generation	SGT	MW_e [MW_{th}]	6.87 [17.18[a]]
	Nuclear process heat		MW_{th} [MW_e]	14.5 [5.8[b]]

gas turbine power generation, and the nuclear process heat. The electrical topping heater consumption has decreased since the steam can be heated to higher temperature. With the removal of the primary heating source for the anode air, more energy is recovered from the hot sweep gas before going through the sweep gas turbine (SGT). This lowers the power generated in the SGT. While the nuclear heat required for both systems are similar, the Natrium system is only heating the incoming water to the HTE cathode while the NuScale system is heating both water and air entering the HTE.

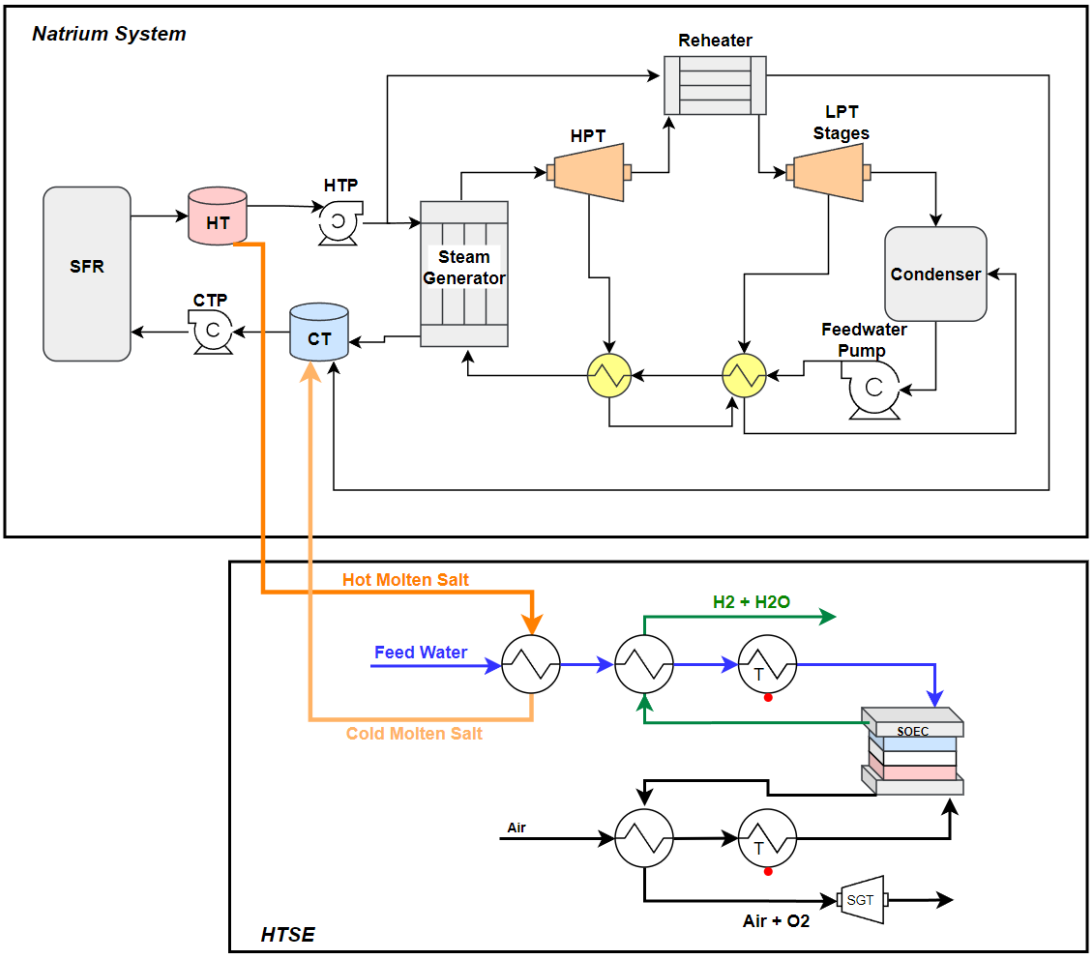

Fig. 3.8: Natrium coupled with HTE baseline. No heat recovery from the hydrogen production.

3.5.1 Configuration 1 Design

Like the baseline Natrium system, the first configuration shown in Fig. 3.9 uses molten salt as the primary heat source for the HTE. In addition, it harnesses the heat from the hydrogen product to preheat the feedwater in the Rankine cycle. This feedwater, initially at 40 °C, is heated to 230 °C before re-entering the Rankine cycle. Preheating a portion of the feedwater contributes to an increase in the thermal efficiency of the Natrium system. By reducing the rate at which steam is bled from the turbines to preheat the feedwater, the

system achieves greater efficiency. Under this configuration, approximately 5-15% of the feedwater can be preheated using the HTE waste heat depending on operating conditions of the Natrium power cycle and hydrogen production rate. With this configuration the hydrogen product is cooled and separated close to 70 °C.

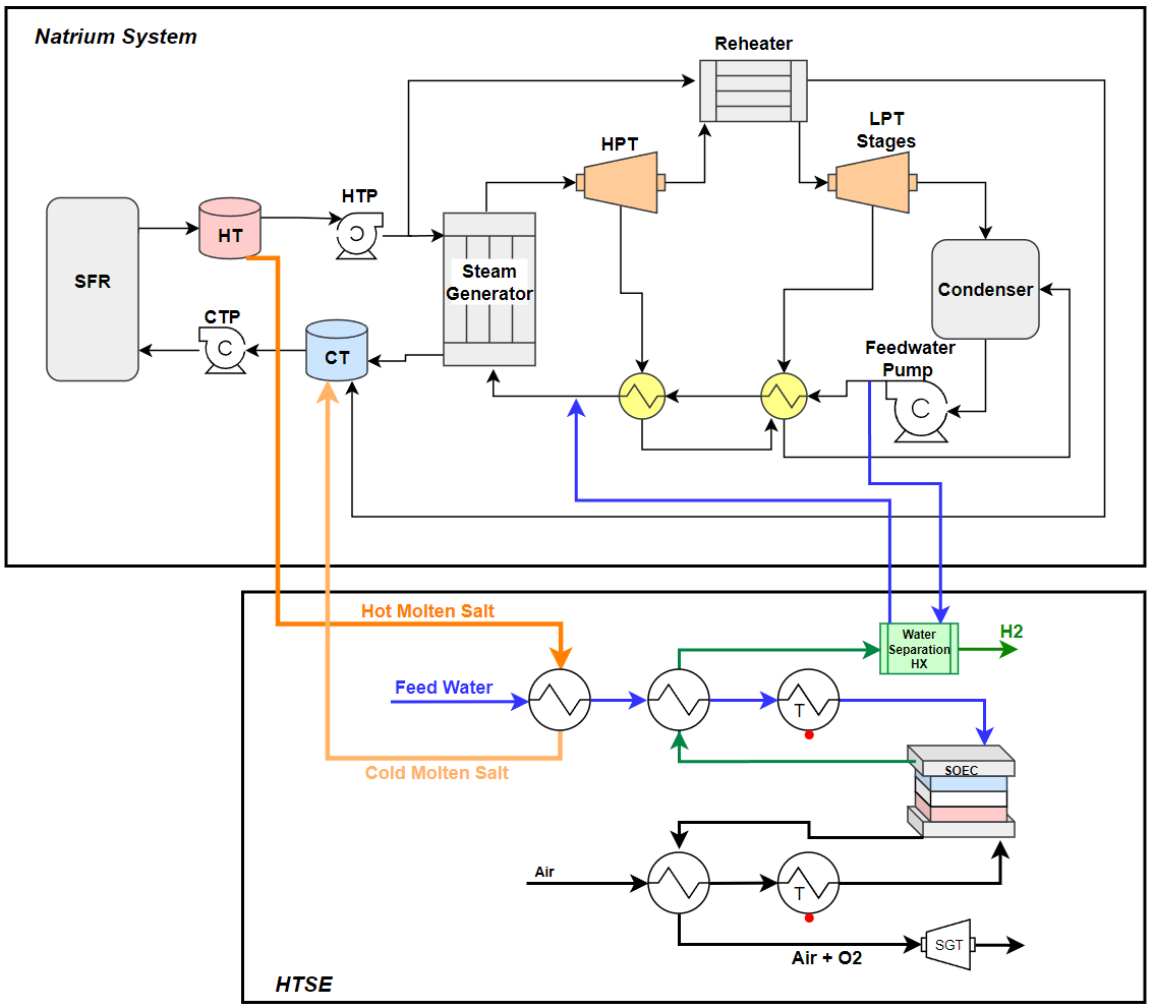

Fig. 3.9: Configuration 1: Natrium with HTE thermally coupled with Rankine feedwater preheating.

3.5.2 Configuration 2 Design

The second configuration, shown in Fig. 3.10, has similarities to the first configuration, utilizing molten salt as the primary heat source in the HTE. However, in this configuration, heat is recovered from the hydrogen product at two distinct points.

Initially, steam from the Rankine cycle is bled after the first turbine stage and is subsequently reheated using the hydrogen product in the HTE. This steam, bled at 237 °C, undergoes reheating to 480 °C utilizing the heat from the hydrogen product. This initial heat exchange does not completely separate the steam from the hydrogen product stream, and the hydrogen mixture exits this heat exchanger at 260 °C, with the saturation temperature of the steam at 17.3 bar being 205 °C. To recover more heat from the hydrogen product (cathode) stream and separate steam from hydrogen, a second heat exchanger is employed, utilizing feedwater from the Natrium cycle to cool the fluid. This process not only ensures complete cooling and separation of the hydrogen but also elevates the temperature of the feedwater to 230 °C, thus increasing the thermal efficiency of the Natrium system.

This configuration is designed to have smaller temperature differences in the heat exchangers, offering advantages by reducing entropy generation. By effectively reducing the heat input to the reheat process, this configuration is anticipated to increase the thermal efficiency of the Natrium system. The HTE has the capacity to reheat approximately 10% of the steam, indicating the potential efficiency gains achievable through this heat recovery approach.

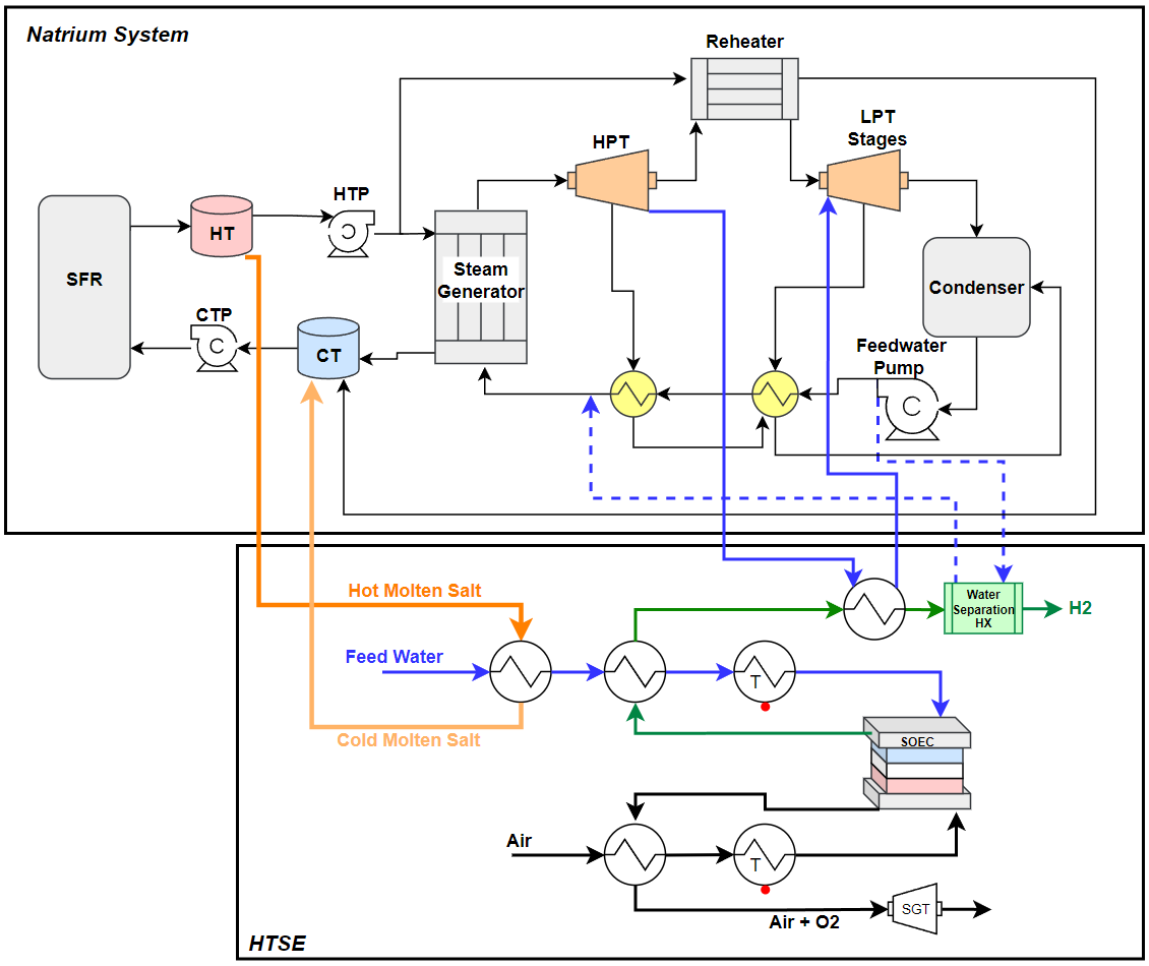

Fig. 3.10: Configuration 2: Natrium with HTE thermally coupled with Rankine reheat and feedwater preheating.

3.5.3 Configuration 3 Design

The third configuration shown in Fig. 3.11 will use lower-grade steam directly from the turbines to feed the HTE system and produce hydrogen in the stack. The molten salt TES loop will not be used to heat the cathode and anode sources, which significantly reduces the complexity of the integrated system (i.e. Natrium IES). The cathode steam source will be bled directly from the Natrium rankine cycle after the first turbine stage at 237 °C. The anode source (air) is preheated using hot sweep gasses exiting the stack. Makeup water

will be preheated using the produced hydrogen product and merged back into the Natrium model. This configuration reduces the number of heat exchangers where boiling occurs and reduces complexity of the HTE model. This configuration may not affect the thermal efficiency of the Natrium system as much as the other two configurations, however, it may be more cost effective because it does not need molten salt heat exchangers to heat input fluids.

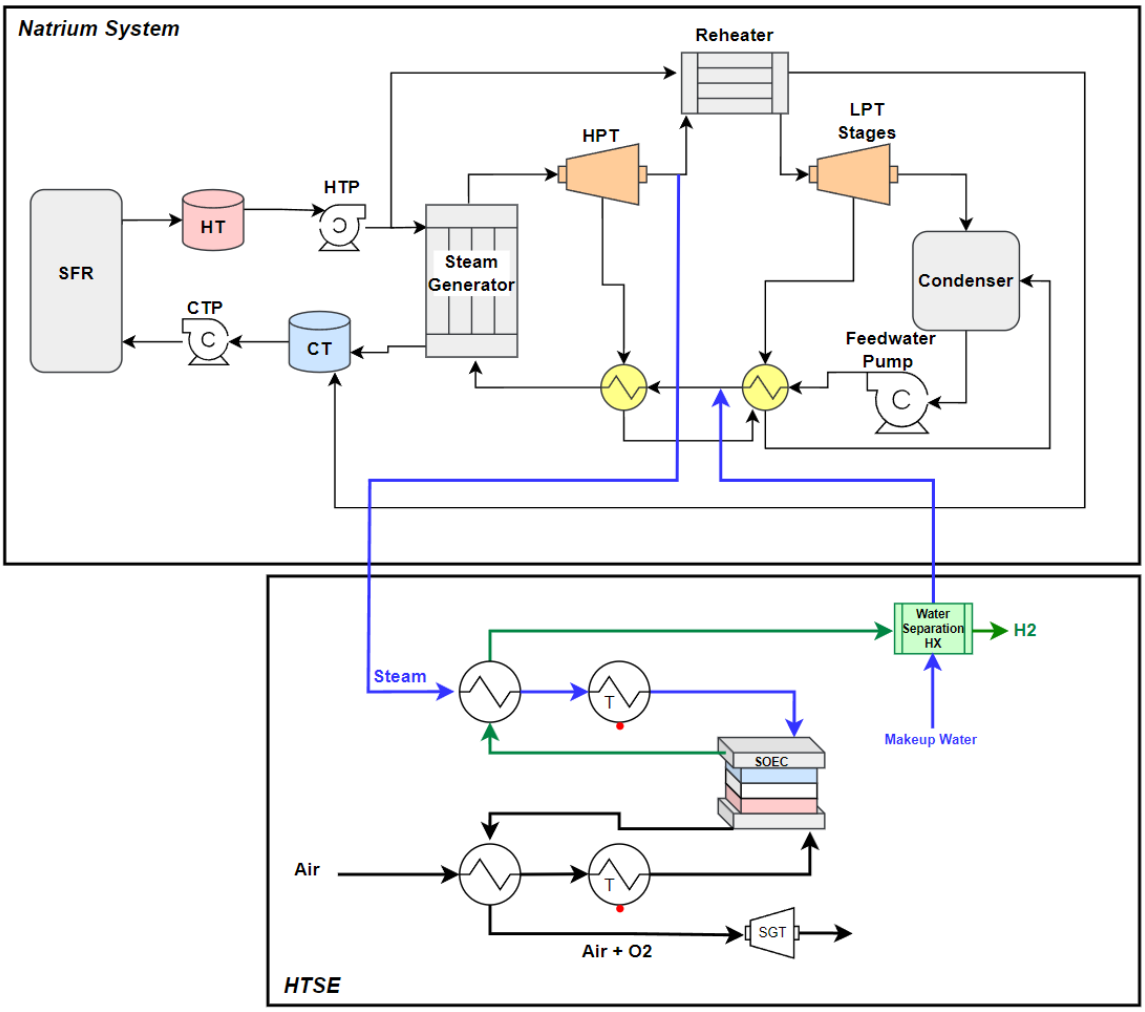

Fig. 3.11: Configuration 3: Natrium coupled with HTE using steam directly from the turbines and preheating makeup water. No SGT in this configuration.

3.5.4 Performance Metrics

These three configurations will be modeled and simulated in Dymola. The thermal efficiency of each configuration will be compared to the baseline Natrium system coupled with hydrogen production (no heat recovery). The thermal efficiency of the Natrium system is calculated as,

$$\eta_{natrium} = \frac{W_e - W_{pumps}}{Q_{boiler} + Q_{reheat}} \tag{3.9}$$

where W_e is the electrical power output, W_{pumps} is the power required to operate the pumps, Q_{boiler} is the heat input to the boiler, and Q_{reheat} is the heat input to the reheater. Pump work will be calculated via,

$$W_{pump} = \dot{m} v \Delta P \tag{3.10}$$

where $\dot{m}$ is the mass flow rate, v is the specific volume of water, and ΔP is the pressure increase. The heat input to the boiler and reheat will be calculated using the temperature change of the molten salt in the boiler and reheater,

$$Q = \dot{m}_{salt} c_p (T_{in} - T_{out}). \tag{3.11}$$

The operating conditions (demand) of the Natrium and HTE systems change how much thermal energy can be recovered from the hydrogen production and how much the recovered heat effect the thermal efficiency of the Natrium system.

The performance of the HTE process can be defined as the heating value of the produced hydrogen divided by the total equivalent thermal energy (combining both thermal and electrical energy) required to produce it [47],

$$\eta_{HTE} = \frac{LHV}{\sum_i Q_i - Q_{SGT}} \tag{3.12}$$

where LHV is the lower heating value (LHV) of hydrogen multiplied by the mass flow rate of hydrogen produced. The LHV of hydrogen at 25°C is 119.96 MJ/kg. The denominator sums all energy that is consumed in the process and subtracts the thermal equivalent of electricity generated in the sweep gas turbine (Q_{SGT}). Q_i includes, thermal energy from the molten salt and thermal equivalent energy of any electrically driven component such as pumps, compressors, electrolyzer, and electrical topping heaters.

In order to evaluate the combined efficiencies of the Natrium BOP and hydrogen generation in the HTE, the following overall efficiency will be used:

$$\eta_{overall} = \frac{(W_{net}/\eta_{natrium}) + LHV}{Q_{MS}} \tag{3.13}$$

This equation combines the thermal efficiency of the Natrium system and hydrogen production efficiency in the HTE. Q_{MS} refers to the energy that is utilized from the molten salt energy storage. This energy is used in both the Natrium power cycle and hydrogen production. W_{net} is the available energy to the grid. When $W_{net} = 0$, all electricity generated by the Natrium steam cycle is being used to produce hydrogen which is captured in the LHV term.

3.6 Hydrogen Storage Integration

In applications where low pressure hydrogen is not directly utilized, hydrogen produced from the HTE will undergo compression and storage within a salt cavity. To enhance energy efficiency during compression, a multi-staged compression approach is employed, utilizing Natrium feedwater to cool hydrogen between compression stages. The compression system, shown in Fig. 3.12, has three compressors and three intercooling heat exchangers. An ideal multi-stage compression system cools the fluid to the initial temperature, T_1 at each intercooler.

Using the ideal gas assumption the optimal interstage pressures can be calculated. Pressure at the inlet and outlet (P_1, P_6) of the multi-stage compression system are known and assuming constant pressure cooling in the intercoolers, the pressures at P_2 and P_4 can

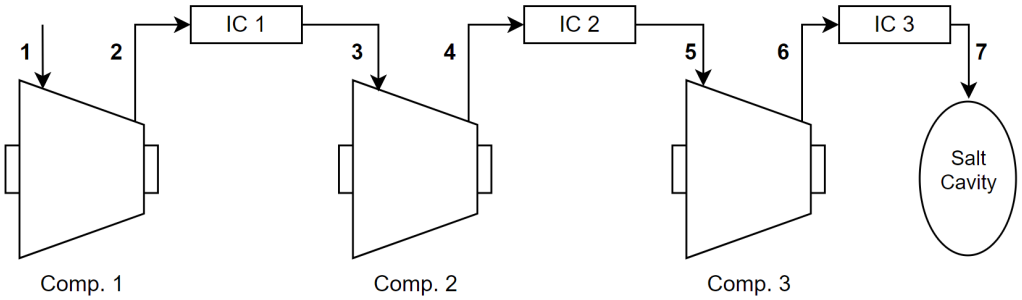

Fig. 3.12: Hydrogen storage diagram.

be optimized. Equations 3.14 and 3.15 [48] solve for the optimized interstage pressures, which results in all three compressors having an equal compression ratio.

$$P_{2,opt} = \theta_{IC2}^{1/(3\gamma)} \theta_{IC1}^{1/(3\gamma)} P_1^{2/3} P_6^{1/3} \tag{3.14}$$

$$P_{4,opt} = \left(\frac{\theta_{IC2}^{2/(3\gamma)}}{\theta_{IC1}^{1/(3\gamma)}} \right) P_1^{1/3} P_6^{2/3} \tag{3.15}$$

$\theta_{IC1} = \frac{T_3/\eta_{isen2}}{T_1\eta_{isen1}}$, $\theta_{IC2} = \frac{T_5/\eta_{isen3}}{T_1\eta_{isen1}}$, if the isentropic efficiency is constant and the same for all three compressors than the θ simplifies to a ratio of temperatures, and $\gamma = (k-1)k$ where k is the ratio of heat transfer coefficients which for hydrogen, $k = 1.405$.

The incorporation of water for hydrogen cooling between compression stages provides additional thermal coupling between the Natrium system and hydrogen production and storage. The hydrogen will be compressed up to 150 bar for salt cavity storage. All three compressors will have a isentropic efficiency of $\eta_{isen} = 0.86$ and the intercoolers will cool hydrogen to 50°C between each compressor stage.

Hydrogen storage in salt cavity will be represented by Eq. 3.16,

$$\frac{dH}{dt} = \dot{H}_{in} - \dot{H}_{out} \tag{3.16}$$

where H is kg of Hydrogen stored, $\dot{H}_{in}$ is the rate of hydrogen at storage inlet, and $\dot{H}_{out}$ is the rate of hydrogen at storage outlet. The Dymola model will integrate this equation for the instantaneous level of hydrogen storage during simulation.

3.7 Optimization and Case Study

Once the dynamic model of the Natrium IES with hydrogen production and storage is completed, the system will undergo optimization for various energy markets. Prospective energy markets include Texas (ERCOT), California (CAISO) and mid-western states (MISO). The system optimization will be conducted using Idaho National Laboratory's Holistic Energy Resource Optimization Network (HERON). HERON is an effective tool for performing techno-economic analysis (TEA) and providing uncertainty quantification for systems interfacing with multiple resource markets (electricity, heat, and hydrogen) [49].

HERON uses a two layer optimization algorithm to execute the stochastic TEA, as shown in Fig. 3.13. The primary objective of the optimization is to maximize the net present value (NPV) of the Natrium system which is influenced by several factors, including weather patterns, resource demands, resource prices, and component sizes and costs. In the inner layer of optimization, the dispatch for a given set of capacities is fine-tuned, and the statistics of the NPV are relayed to the outer layer. The inner loop simulates multiple instances of electricity prices, market demands, and renewable energy production, providing a distribution of NPVs.

The ultimate verification of the optimal capacities and dispatches will be conducted using the dynamic model implemented in Dymola. This integrated approach ensures a robust optimization process that considers the dynamic behavior of the Natrium system under diverse scenarios, leading to an informed and effective system design for each targeted energy market.

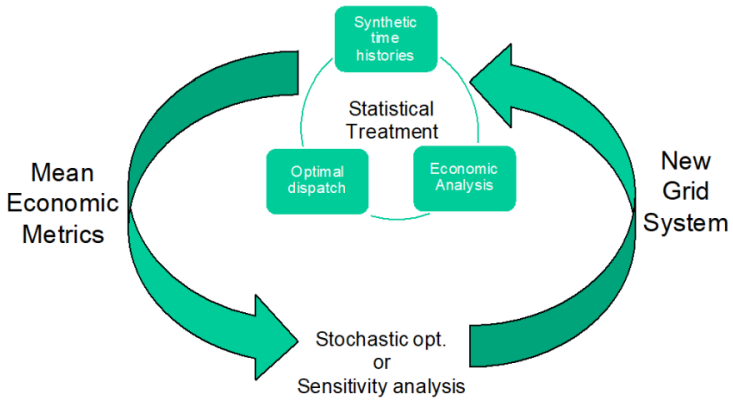

Fig. 3.13: Inner and outer loop workflow of HERON [49].

3.8 RAVEN

Due to the unpredictability and uncertainty of the electricity grid, weather, load, and market conditions that drive the economics of energy systems, RAVEN treats these inputs as stochastic systems which can be implemented using a sampling technique. RAVEN produces synthetic time series with fundamentally consistent behavior while still retaining statistical independence [21]. In other words, raven can sample from a distribution of potential market scenarios in order to calculate economic parameters, such as NPV, while also quantifying uncertainty.

For this thesis work the only stochastic variable which will be modeled is the electricity price. The US energy market can be classified into two categories: regulated and deregulated. Regulated markets have grid operators who also act as electricity suppliers. Power generation, transmission, and distribution is all done with a single integrated utility. State leadership will oversee the utilities and decide how much capacity to procure from the power utilities, but the utilities decide how to produce that energy [21].

3.8.1 Synthetic Time Series Modeling

The synthetic time series models for the electricity price are trained and modeled using RAVEN from Idaho National Lab. The training process consists of two main steps: detrending the signal using Fourier analysis to remove strong patterns and then characterizing the residual noise using auto regressive moving average (ARMA) algorithm [50].

3.8.2 Fourier Analysis

The fourier detrending is used to remove patterns, such as, every 12 and 24 hours the electricity price tends to rise and fall periodically with those time scales. The ARMA algorithm requires random noise that is stationary (the mean and variance are constant) and normally distributed. The Fourier series can be used to remove individual frequencies from the signal [50],

$$F = \sum_{c} \sum_{i=0}^{k} a_i \sin\left(\frac{2\pi f_i}{c} t\right) + b_i \cos\left(\frac{2\pi f_i}{c} t\right) \tag{3.17}$$

where c are a set of characteristic time periods with strong periodical patterns (ex: 12, 24 hours), f_i are integer frequencies, and a_i and b_i are calculated to fit F to the original signal.

This remaining signal with random noise may not have a normal distribution required for the ARMA algorithm. Therefore, the remaining noise is passed through a transformation to convert the residual into a standard normal distribution,

$$y = \Phi^{-1}[f(x - F)] \tag{3.18}$$

where Φ is a normal distribution cumulative distribution function (CDF), f is the empirical cumulative distribution of the Fourier-reduced signal, x is the original signal, F is the signal with seasonal Fourier frequencies removed, therefore, $x - F$ is the detrended signal, and y is the transformed, normalized, residual signal [50].

3.8.3 ARMA Algorithm

With a normalized, residual signal from the original historical price signal the ARMA algorithm can be used to model the residual noise. The ARMA algorithm is a combination of autoregressive (AR) and moving average (MA) models. The two models are added together to form the following equation [50],

$$y_t = \sum_{i}^{p} \phi_i y_{t-i} + \epsilon_t + \sum_{j}^{q} \theta_j \epsilon_{t-j} \tag{3.19}$$

where p is the maximum number of AR lag terms, ϕ_i is the linear extrapolation term, ϵ_t is the residual noise, q is the maximum number of MA lag terms, and θ_j is the moving weight associated with the MA lag term. The ARMA model is fitted to maximize a likelihood function.

It is important to note, the ARMA model is only valid for stationary data. It is important to ensure Fourier detrending and normalization results in stationary residual noise. Figure 3.14 shows an example of the Fourier detrending and ARMA modeling process. The blue line shows the original signal (electricity demand), the orange line shows the Fourier signal that will be removed from the original signal leaving the green remaining noise. Then the red line shows the remaining noise after being transformed to a normal distribution with the mean at y=0.

The process described above removes seasonal trends from the original signal and transforms the residual to fit a normal distribution. The transformed residual is used to find ARMA model parameters ϕ_i and θ_j. Scenarios can be generated by using an inverse transformation and adding previously removed Fourier frequencies back into the sample,

$$x_t = f^{-1}[\Phi(y_t)] + F. \tag{3.20}$$

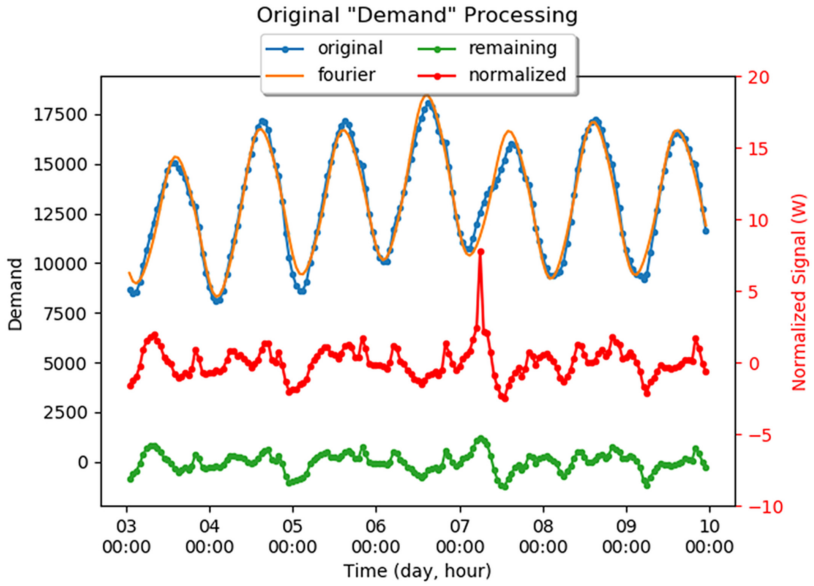

Fig. 3.14: Fourier detrending and ARMA modeling process [50].

3.8.4 TEAL

As shown in Fig. 3.13, there is an economic analysis as part of the inner loop. HERON uses a plugin called TEAL (Tool for Economic AnaLysis) which has the capability to calculate the Net Present Value (NPV) with HERON and RAVEN. The plugin uses cashflows from the HERON simulation. TEAL also has flexible options to include taxes, inflation, discount rates and combine cashflows from different components with different component life time durations [51]. The NPV is calculated using the following equation,

$$NPV = \sum_{y=0}^{N} \frac{CF_y}{(1 + DiscountRate)^y} \tag{3.21}$$

which sums over the years y=0 to N where N is the least common multiple of all component lifetimes involved so all components will reach end of life at the same time. CF_y are the sum of all cash flows which account for capital cost, operation and maintenance costs, and revenue generated for every component during simulation, $DiscountRate$ is the rate of interest used to discount all future cash flows due to time value of money.

In order to decrease runtime, all costs associated with components in the Natrium system will be scaled to a single year cost. For operation and maintenance costs, this is already done as values are typically reported as annual or hourly operation costs. For capital costs, the costs will be scaled to a single year cost using the capital recovery factor (CRF) which is calculated using the following equation,

$$CRF = \frac{r(1+r)^n}{(1+r)^n - 1} \tag{3.22}$$

r is the discount rate, n is the number of years the component will be in operation. For discount rate of 8% and 30 year component life, the CRF is 0.088. The capital cost will be multiplied by the CRF to get the single year cost. Simulating the HERON model with 1 year scaled costs compared to 30 year full scale costs will yield the same optimal capacities and dispatches because the electricity prices being sampled in both scenarios will come from the same distribution. The NPV values will be scaled down for the 1 year lifetime simulations.

3.8.5 HERON Model

Figure 3.15 shows the components and resources in the HERON model. HERON simulates operation by managing the production, consumption, and storage of resources. For the Natrium design the three resource are: Heat, Electricity, and H2. Each blue circle in Fig. 3.15 is a component that consumes, produces, or stores a resource. The nuclear power plant (NPP) produces heat that can be used to produce electricity in the balance of plant (BOP), also known as the steam cycle, go into storage in the thermal energy storage (TES), or go the high temperature electrolysis (HTE) to produce hydrogen. The electricity produced in the BOP can be used to produce hydrogen in the HTE or go into the grid. The hydrogen produced in the HTE can be stored in the hydrogen storage or go into the H2 market. Table 3.5 shows the components, dispatch type, their associated resources capacities, and efficiency. Components with a fixed dispatch will always produce/consume the specified

amount of a resource. Independently dispatched components vary production/consumption based on system dispatch optimization.

Table 3.5: HERON model components, dispatch, capacities, and efficiency.

Component	**Dispatch**	**Capacity**	**Efficiency & Inputs**
NPP	Fixed	0.8625 GW_{th}	
TES	Independent	2.288 GWh_{th}	
BOP	Independent	0.2 - 0.5 GW_e	40%
HTE	Independent	7970.4 kg/hr	0.3269 GW_e, 0.0783 GW_{th}
H2 Storage	Independent	40000 kg	
Grid	Independent	∞	
H2 Market	Fixed	6500 kg/hr	

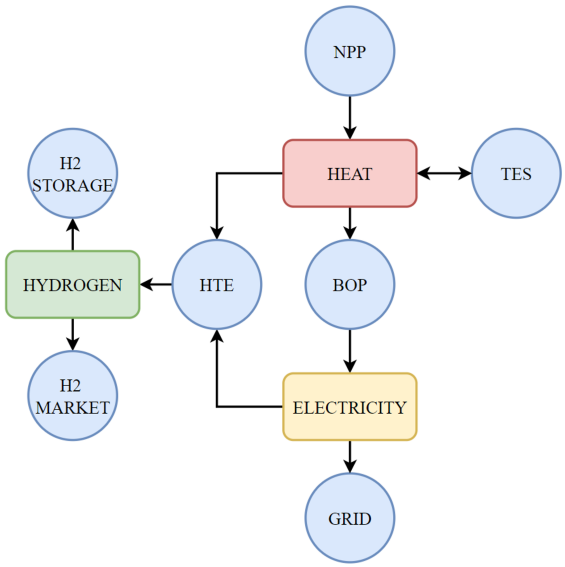

Fig. 3.15: HERON model components and resources.

3.8.6 Cost Parameters

Each component in the HERON model requires economic parameters for the simulation. These include: capital cost, variable operation and maintenance (VOM), and fixed operational and maintenance (FOM). Table 3.6 shows each component cost utilized in the HERON model to calculate NPV. Each capital cost is scaled using the CRF and its total cost is reported in Tab. 3.6.

Table 3.6: HERON model component costs.

System Cost	**Single Year Cost**	**Total Cost**	**Units**	**Reference**
NPP Capex	113.117E+06	1330E+06	$\$/GW_{th}$	[52]
NPP FOM	44.8E+06		$\$/GW_{th}$	[52]
NPP VOM	7.43E+03		$\$/GWh_{th}$	[52]
BOP Capex	61.11E+06	6.00E+06	$\$/GW_{e}$	[53]
BOP FOM	50.0E+06		$\$/GW_{e}$	[53]
BOP VOM	1.00E+03		$\$/GWh_{e}$	[53]
TES Capex	0.600E+06	6.75E+06	$\$/GWh_{th}$	[53]
TES FOM	28.5E+03		$\$/GWh_{th}$	[54]
TES VOM	4.00E+03		$\$/GWh_{th}$	[54]
HTE Capex	2690.53	30.574E+03	$\$/kg/h\ H2$	[55]
HTE FOM	32.6E+06		$\$/GW_{e}$	[55]
HTE VOM	0.1398		$\$/kg/h\ H2$	[55]
H2 Storage Capex	3.344	38	$\$/kg\ H2$	[56]

The salt cavity hydrogen storage cost is for a site with a capacity of 500-tons of hydrogen which is equal to 500,000 kg. For the HERON simulations in this study, it is assumed to be scaled on a per Natrium size. In the results section the hydrogen storage capacities will be on the order of 40,000 kg of hydrogen in capacity, therefore to utilize a salt cavity of 500-tons ∼10 Natrium systems would be needed.

Capex is the capital cost for the component or the overnight investment cost. FOM is the fixed operation cost typically calculated based on the capacity of the component once per year. The VOM varies based on the operation and usage of the given component.

CHAPTER 4

RESULTS

This chapter discusses the results from modeling and simulating the configurations of Natrium coupled with HTE using Dymola as discussed in the previous chapter. The stochastic bi-level capacity and dispatch optimization using HERON is also discussed. Three independent system operators (ISO) will be used to represent the three regions in the United States. The ISOs are the California Independent System Operator (CAISO), the Electric Reliability Council of Texas (ERCOT), and the Midcontinent Independent System Operator (MISO). The results will be presented in two sections. The first section will discuss the results from the Natrium-HTE coupling. The second section will discuss the results from the stochastic bi-level capacity and dispatch optimization.

4.1 Natrium-HTE Coupling

This section will discuss the results from coupling the Natrium system with hydrogen production via high temperature steam electrolysis. Three configurations will be discussed. The first configuration involves the integration of the Natrium system with the molten salt energy storage and feedwater preheating. The second configuration integrates with the molten salt energy storage, feedwater preheating, and steam reheating. The third configuration integrates by utilizing steam directly from the steam turbines to supply H2O to the HTE system. The results will be presented in the following order: configuration 1, configuration 2, and configuration 3. Many plots will compare simulation results from the configurations with the baseline Natrium system which does not integrate with the HTE system and only produces electricity.

4.1.1 Input Profiles

The analysis of each of the three configurations will use the same specified input profiles outlined in Fig. 4.1. These simplified input profiles will span a 24-hour period, allowing observation of the system's performance under several operating conditions. Following a 4 hour initialization period, every combination of maximum/minimum electricity generation and hydrogen production is simulated. Natrium electricity generation operates between 200-500 MW_e and the HTE operates between 0.2-2.214 kg/s (720-7970.4 kg/h). The corresponding electrical power requirement for hydrogen production is between 140.4-286 MW_e. For the input profile in this section the minimum hydrogen production is 0.91 kg/s. The min/max electricity generation for these input profiles is between 286.6-500 MW_e.

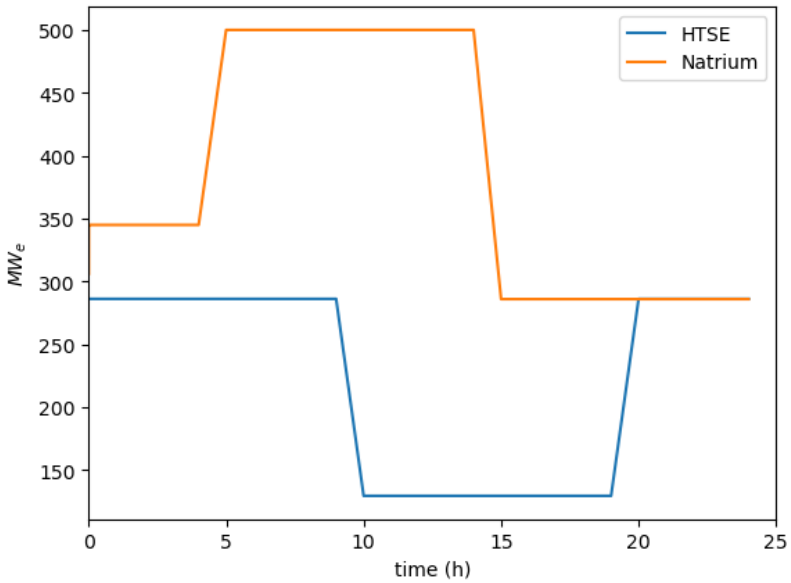

Fig. 4.1: Hourly electricity demands from grid (orange) and HTE (blue).

Varying operating conditions allow for flexible electricity dispatch of Natrium power to the grid. Figure 4.2 shows how much electricity is available to be sent to the electricity grid during the simulation. During hours 9-13 in the simulation, the Natrium system is operating

at its max and the hydrogen production at its minimum, therefore, the power to the grid is maximized at 359.6 MW_e. Hours 20-24 show the Natrium at its minimum and hydrogen production at its maximum which results in no power available to the grid. All three configurations are assuming the thermal energy storage can supply sufficient molten salt to operate these profiles for hydrogen production and Natrium BOP electricity generation.

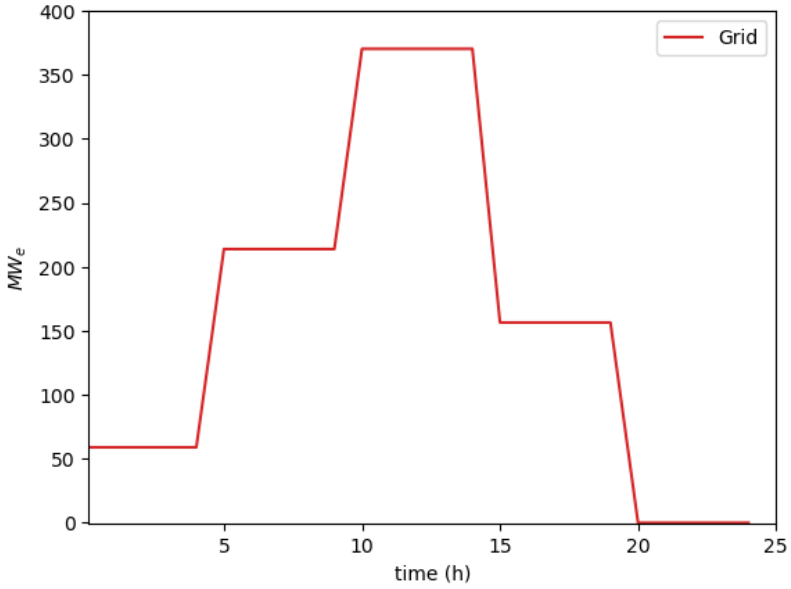

Fig. 4.2: Net electricity available to the grid.

4.1.2 Configuration 1

Configuration 1 integrates the Natrium system with HTE hydrogen production through two fluid streams. The feedwater from the Natrium balance of plant (BOP) cools and condenses the hot hydrogen/steam product generated in the HTE and molten salt from the TES generates steam for the HTE process. Figure 4.3 shows the mass flow rates, temperatures, and heat exchanger sizes for the HTE system in configuration 1 while operating at maximum hydrogen production.

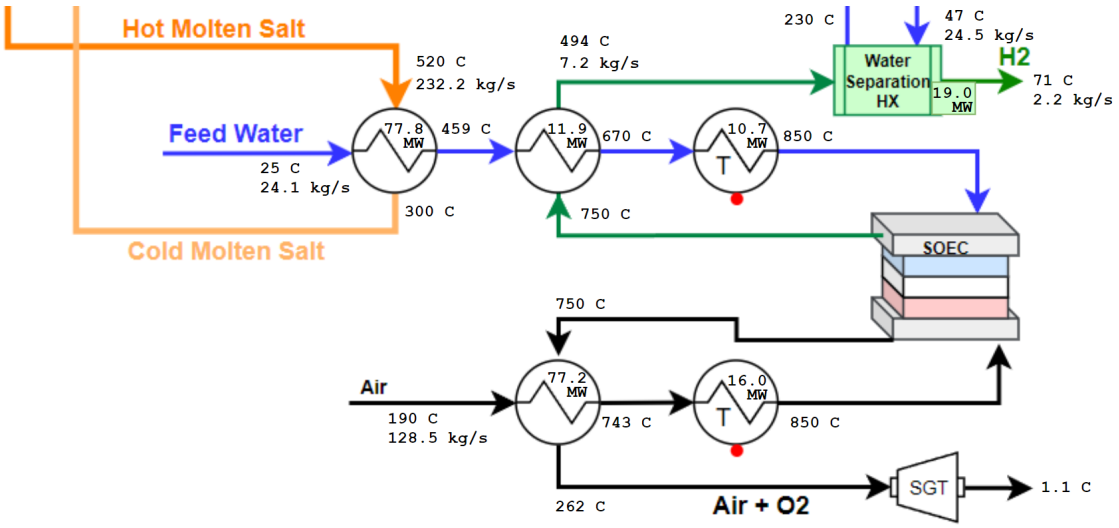

Fig. 4.3: Configuration 1 HTE state points when operating at the maximum hydrogen production rate.

Figure 4.4 shows the amount of heat being recovered from the hydrogen product in the water separation heat exchanger. The amount of heat being recovered is directly proportional to how much hydrogen is being produced. At its peak, the feedwater can recover 19 MWth of energy from the hydrogen product. The heat being recovered in the water separation heat exchanger will reduce heat input in the Natrium BOP and boost thermal efficiency.

In the Natrium BOP, the system bleeds steam from the turbines to preheat feedwater before it enters the steam generator. In this configuration, a portion of that feedwater is being preheated to the design temperature of 230 °C. Therefore, the turbines can bleed less steam depending on how much feedwater is being directed to the HTE system. Figure 4.5 shows the amount of steam being sent to the feedwater regenerators as a percentage of $\dot{m}$ in turbines. A larger percentage shows that more steam is required to preheat the feedwater. The more hydrogen that is being produced, the more feedwater is used to cool, condense, and separate hydrogen product. This results in less steam being bled for the feedwater preheating and more power being generated in the turbines.

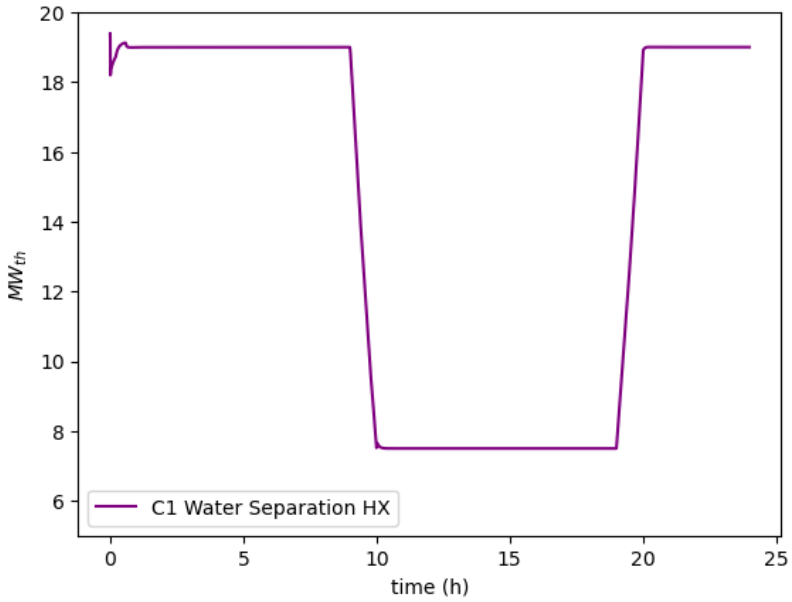

Fig. 4.4: Rate of heat recovered in the cooling and separation of hydrogen product.

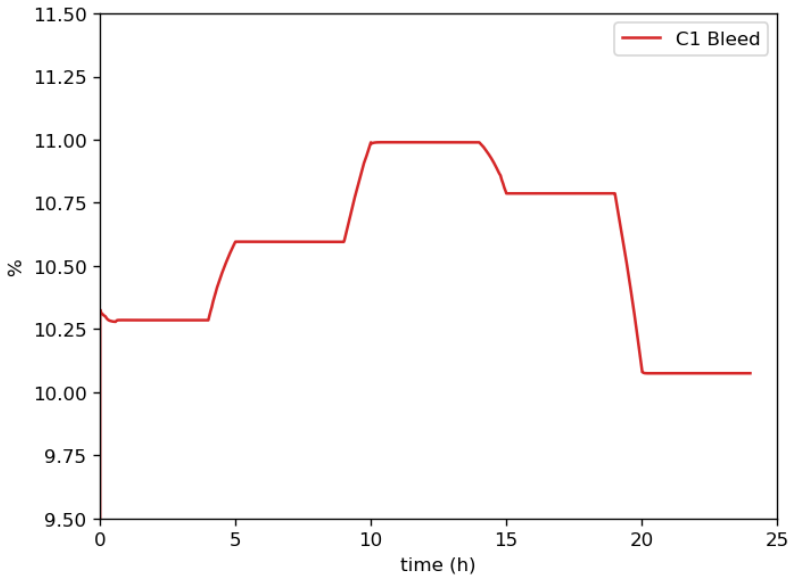

Fig. 4.5: Percentage of steam bled from turbines to feedwater regenerators.

Reducing the amount of steam being utilized to preheat feedwater allows the Natrium system to produce more electricity for the same amount of heat input to the cycle, see Fig. 4.6. This reduction in required heat inputs is going to increase the thermal efficiency.

Figure 4.7 shows the efficiency gains from the Natrium system being coupled with HTE process compared to the standalone Natrium system.

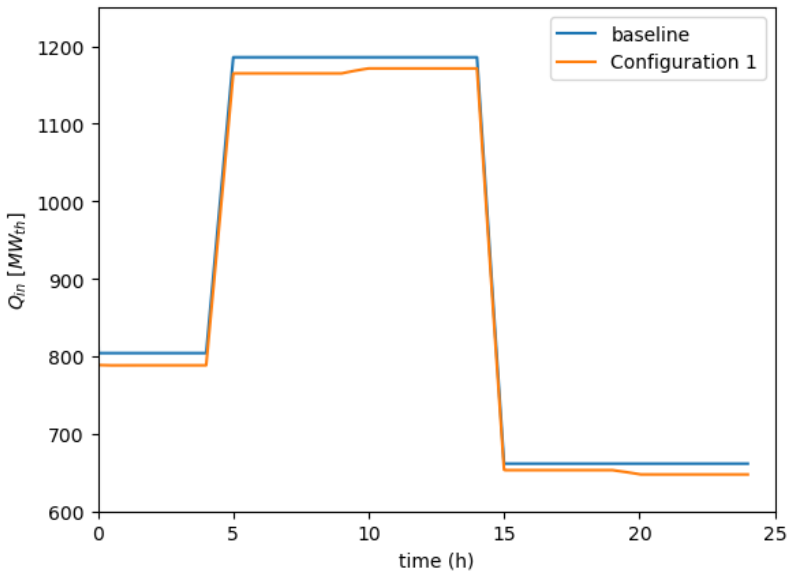

Fig. 4.6: Total heat input to Natrium Rankine cycle. Configuration 1 and baseline Natrium.

The reduction of steam bleeding from the turbines enhances efficiency by up to 0.93%. The most significant improvement in thermal efficiency occurs between hours 20-24, coinciding with Natrium generating minimal electricity and HTE operating at maximum capacity. The ratio of heat recovered in the HTE compared to the total heat going into the steam cycle is maximized during this time period, thus maximizing efficiency gains.

4.1.3 Configuration 2

Configuration 2 utilizes hydrogen product from the HTE to reheat steam and preheat feedwater from the reheat Rankine cycle used in the Natrium system. These results use the same input profiles as shown in Fig. 4.1. The hydrogen product is 494 °C and is used primarily to reheat steam from 230 °C to 480 °C. Figure 4.8 shows the statepoints of the HTE system.

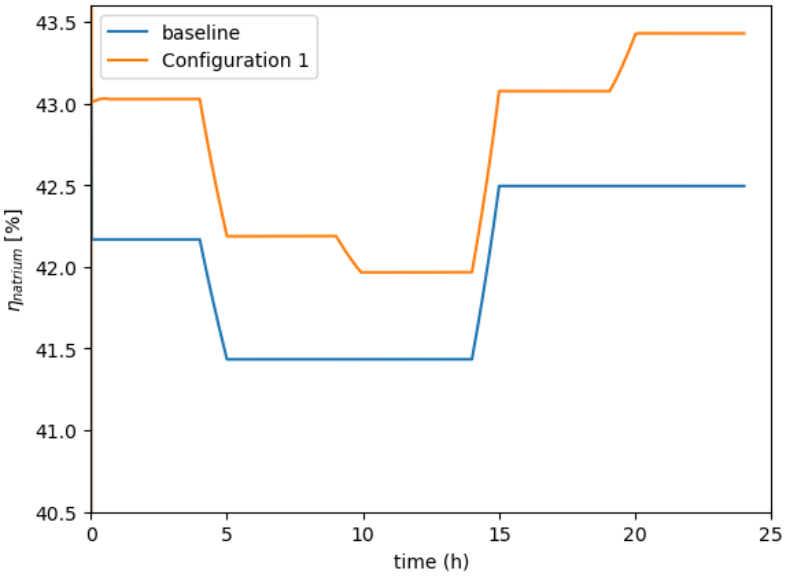

Fig. 4.7: Thermal efficiency of Natrium Rankine cycle. Configuration 1 and baseline Natrium.

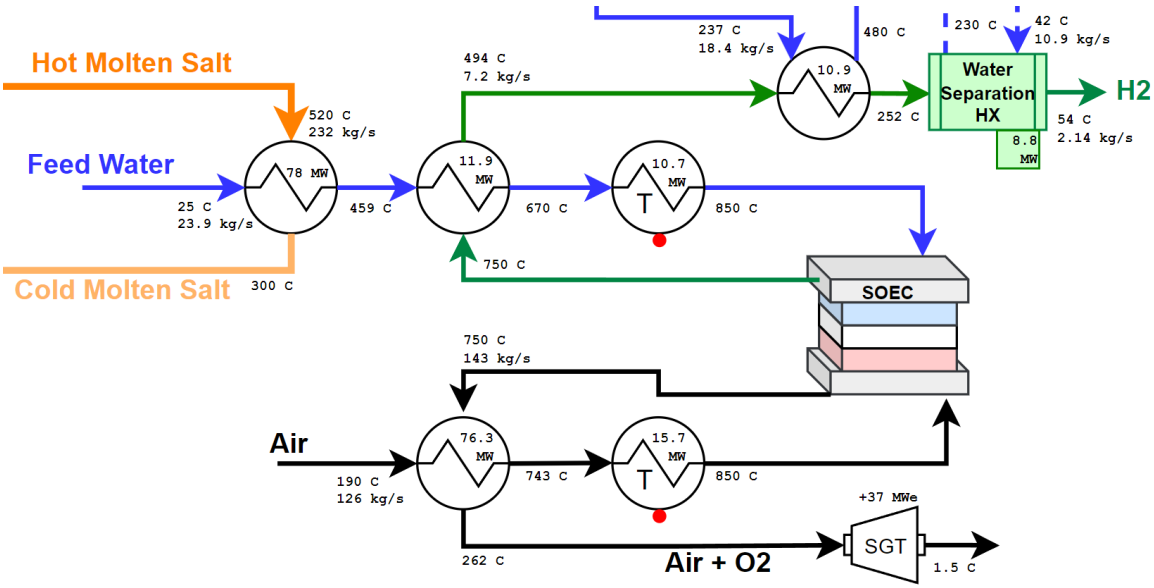

Fig. 4.8: Configuration 2 HTE state points when operating at the maximum hydrogen production rate.

Using the hydrogen product to reheat steam decreases the amount of molten salt required in the reheater to maintain the correct statepoints. This reduction in molten salt required increases the thermal efficiency of the Rankine cycle. Figure 4.9 shows the mass

flow rate of molten salt input to the reheat heat exchanger in the baseline, configuration 1, and configuration 2 models.

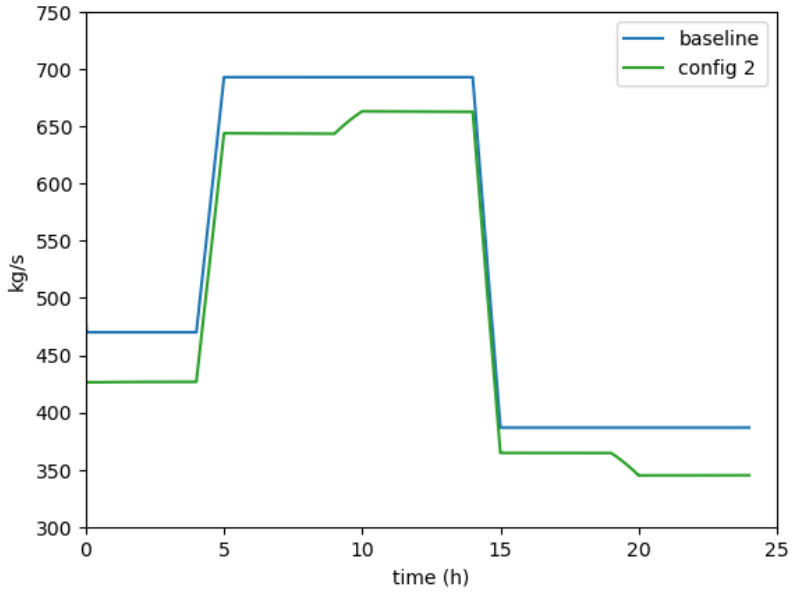

Fig. 4.9: Mass flow rate of molten salt in reheat heat exchanger.

The HTE coupling results in a reduction of 50 kg/s of molten salt between hours 5-9 and 20-24 which is a 7% and 12.5% reduction respectively. When the HTE is operating at its maximum capacity, the reheater heat rate is reduced by 11 MW_{th}. This results in a thermal efficiency boost for the Natrium system. Figure 4.10 shows the thermal efficiency of the baseline Natrium system and configuration 2 integration of hydrogen production.

Reducing the amount of molten salt required in the reheater boosts thermal efficiency up to 1.04%. The water separation heat exchanger in configuration 2 is much smaller compared to configuration 1 and does not have a sizeable impact on the thermal efficiency boost for the BOP due to the steam reheat heat exchanger right before it. However, this second heat exchanger is utilized to fully cool the steam/H2 product which is required for separating the steam from the hydrogen and prepare the final hydrogen product for compression

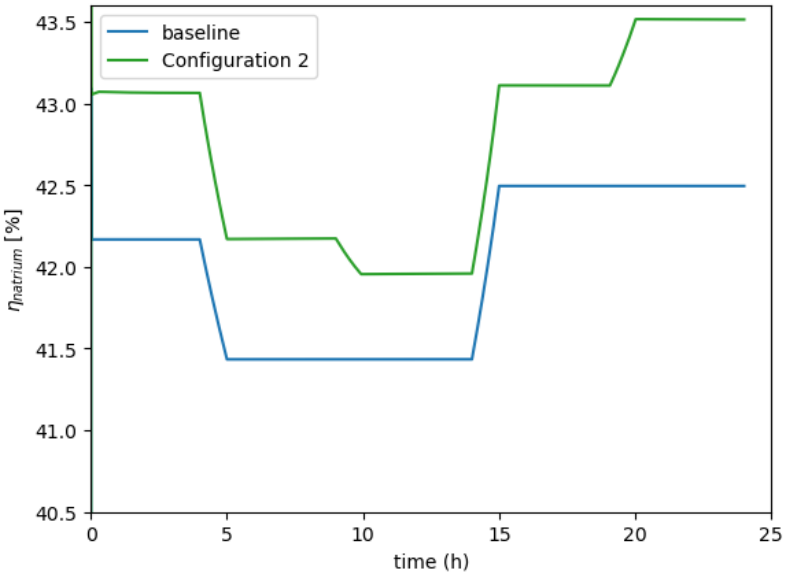

Fig. 4.10: Thermal efficiency of Natrium Rankine cycle. Configuration 2 and baseline Natrium.

and storage. Figure 4.11 shows the heat exchanger size of the first heat exchanger which is used to reheat steam from the BOP, the water separation HX, and the sum of both heat exchangers. The total and water separation HX are dashed in the plot since the steam reheat HX plays the major role in the BOP efficiency boosting. It is interesting to note that although configuration 2 recovers less heat compared to configuration 1 it has a slight edge on BOP efficiency boosting. This is due to the exergy destruction in configuration 1 and will be explored in following sections.

4.1.4 Configuration 3

Configuration 3 directly integrates with the HTE by utilizing steam from the steam cycle as feedstock for the hydrogen production. This configuration does not require the use of molten salt in the hydrogen production, which substantially reduces the complexity of thermal coupling between current Natrium energy island and HTE. Figure 4.12 shows the statepoints of configuration 3 when operating at maximum hydrogen production. One major difference in this configuration compared to the first two is the removal of a steam

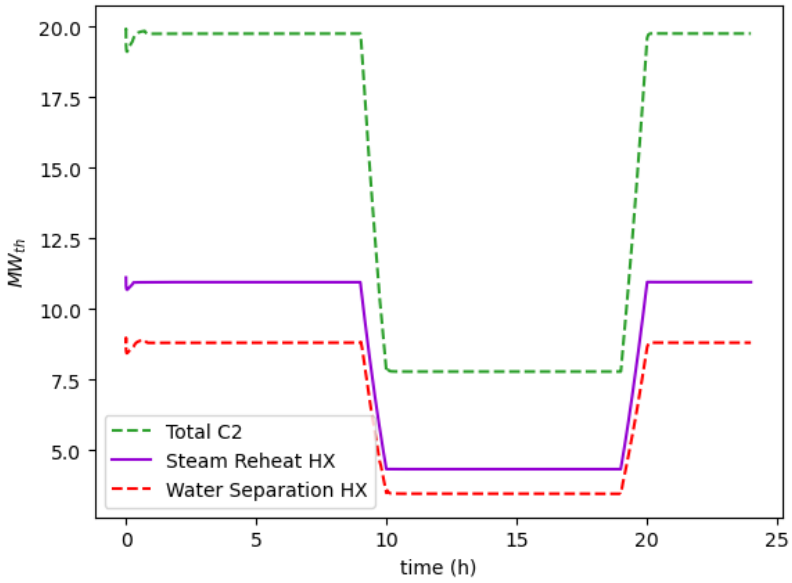

Fig. 4.11: Heat exchanger sizes for configuration 2 heat recovery in HTE. Steam reheat HX, water separation HX, and the total heat rate recovery.

generator in the HTE system which reduces the number of heat exchangers in the HTE system. In addition, the water separation HX is smaller and does not heat the makeup water to the full 230 °C as the other configurations. Although the state points in this system are similar to H2 production with a LWR, the HTE efficiency is different since the large thermal energy input for steam generation is avoided within this HTE configuration.

Figure 4.13 shows the thermal efficiency of Natrium BOP vs the baseline case. The efficiency of Natrium during the simulation of configuration 3 is significantly different from the previous configurations. Increasing hydrogen production results in a lower efficiency than the baseline case due to a significant amount of steam generated in the Natrium energy island is sent to the HTE system. In order to meet the electricity set point, the system will increase its mass flow rate accordingly. This increased mass flow rate will require more heat transfer from the molten salt in the steam generator which results in a decreased Natrium efficiency. However, between hours 10-15 when the hydrogen production rate is reduced, the size of the reheater is smaller compared to the baseline Natrium system which results in

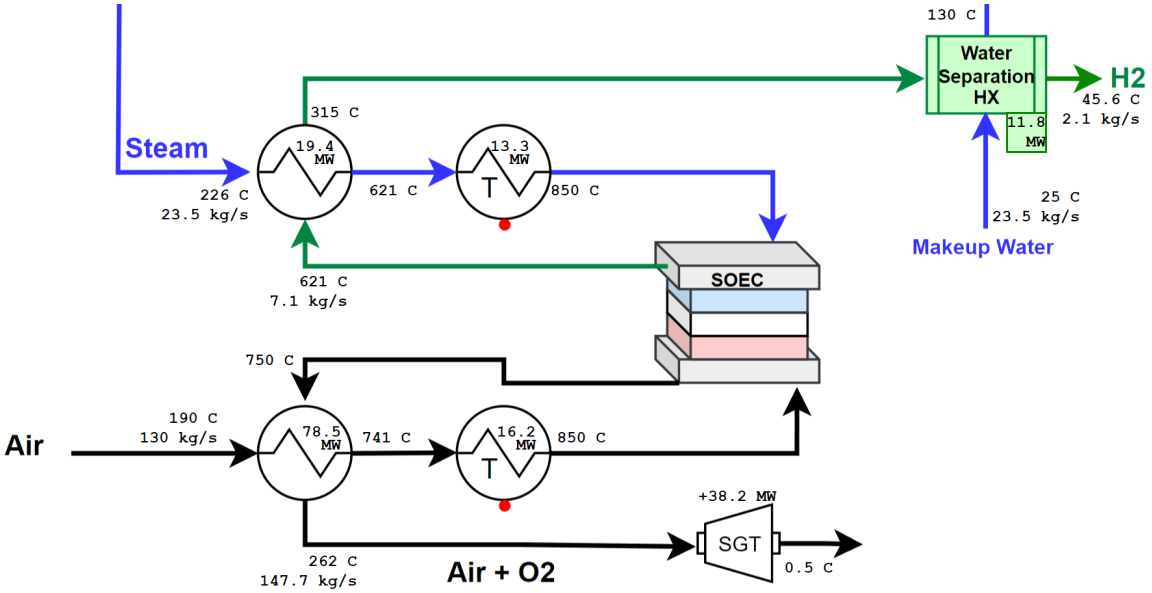

Fig. 4.12: Configuration 3 HTE state points.

a higher efficiency during that time. Figure 4.14 shows the reheater size for configuration 3 and the baseline.

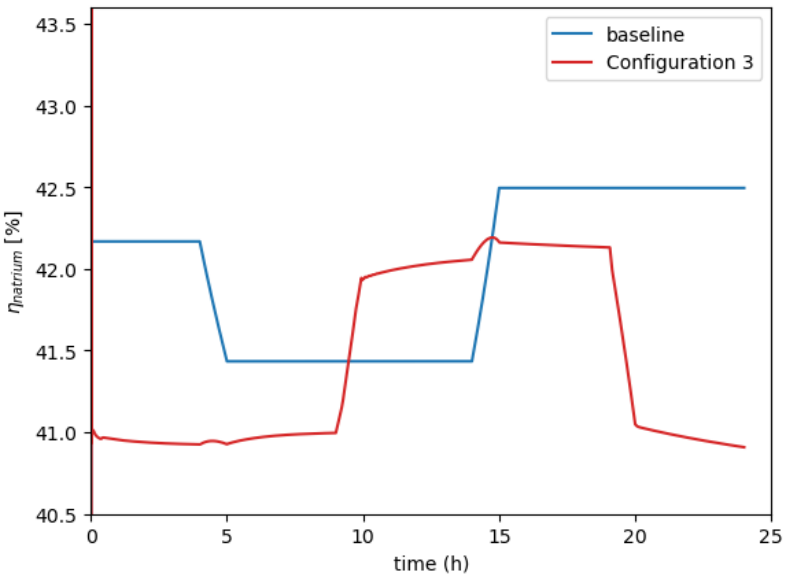

Fig. 4.13: Thermal efficiency of Natrium Rankine cycle. Configuration 3 and baseline Natrium.

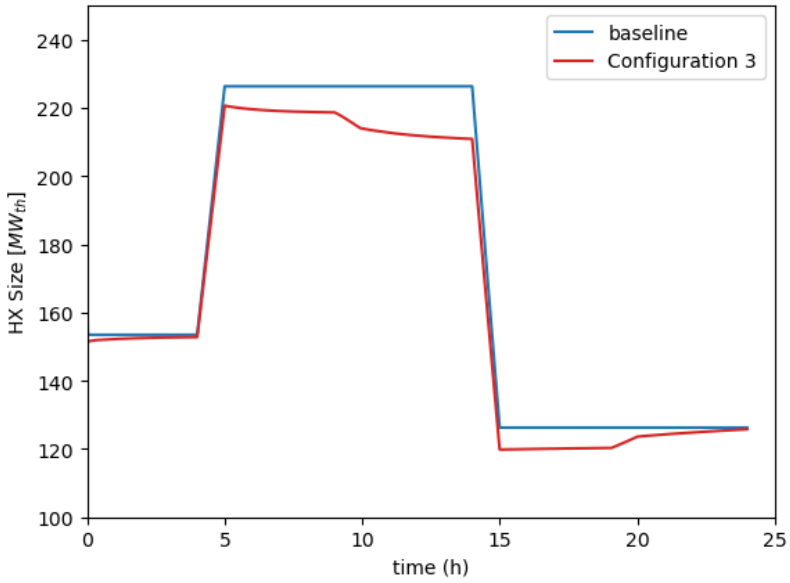

Fig. 4.14: Reheater size for configuration 3 and Natrium baseline BOP.

4.1.5 Dymola Modeling Results and Discussions

Coupling the Natrium nuclear plant with high temperature steam electrolysis can improve the thermal efficiency of the Natrium BOP. Three configurations were explored to couple the two systems. Configuration 1 integrated the Energy Island through the feedwater reheating system. Configuration 2 utilized H2 product to reheat a portion of steam from the BOP Configuration 3 eliminated the steam generator in the HTE system and utilizes steam directly from the steam cycle to feed the H2 system. Figure 4.15 shows the Natrium steam cycle efficiency of all 4 systems simulated in this section.

As shown, configuration 1 and 2 have similar efficiency profiles, however, configuration 2 has a slight improvement during peak hydrogen production phases of the simulation. Configuration 3 sees a reduction in thermal efficiency as steam is being removed from the cycle for hydrogen production. However, as Fig. 4.16 shows, the hydrogen HTE efficiency for configuration 3 is significantly higher than those of the other two configurations. This is due to configuration 3 having considerably less heat input than the other two configurations.

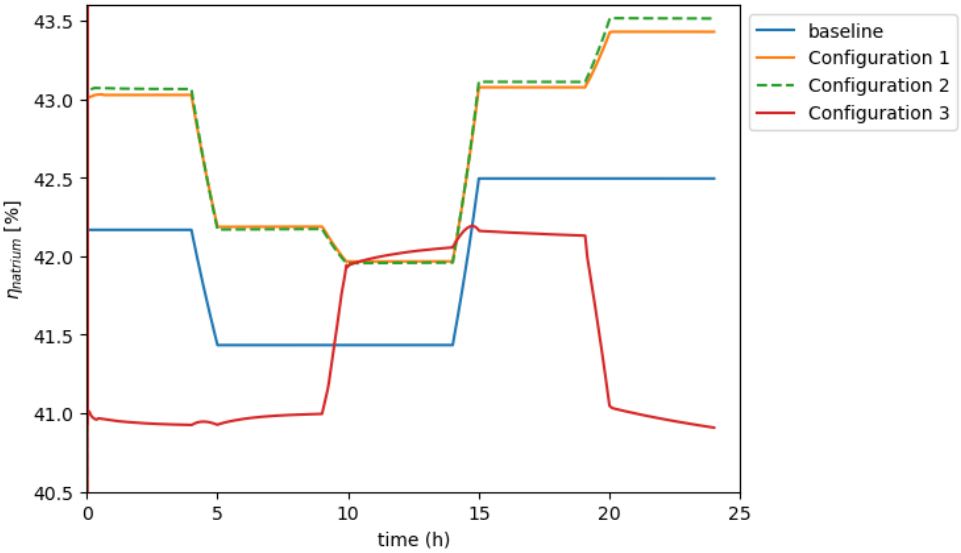

Fig. 4.15: Thermal efficiency of Natrium plant for all 3 configurations and baseline.

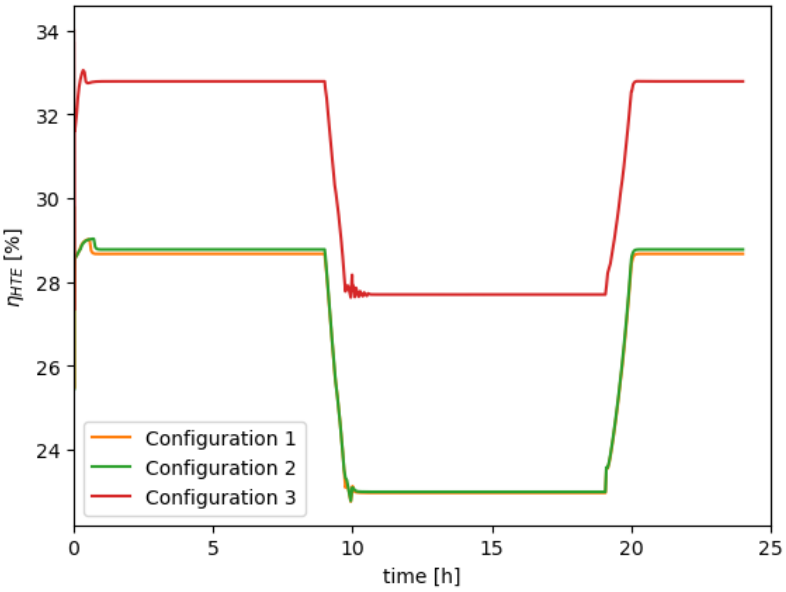

Fig. 4.16: HTE efficiency.

In order to evaluate all three configurations electricity generation and hydrogen production coupled together, Fig. 4.17 shows the overall efficiency which combines Natrium steam cycle thermal efficiency and HTE hydrogen production efficiency.

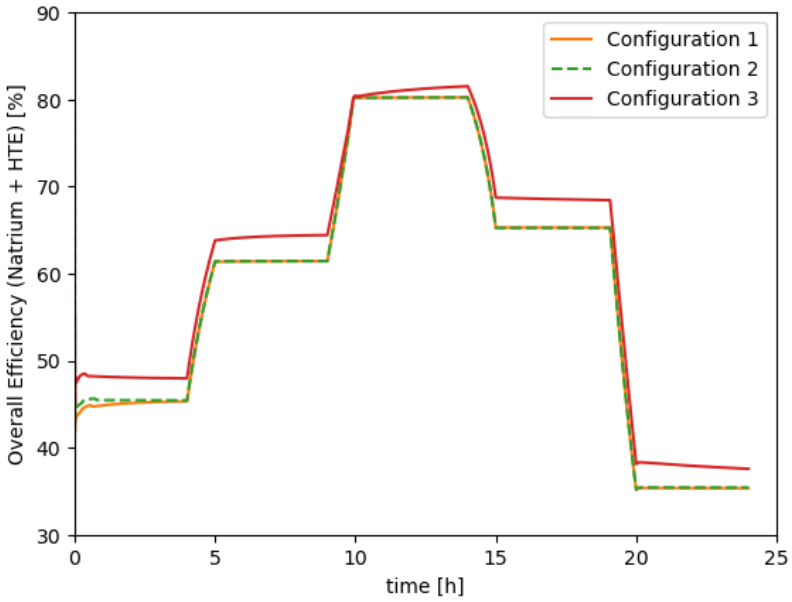

Fig. 4.17: Overall system efficiency for all three configurations.

The shape of these overall efficiency curves follow the net electricity available to the grid profile as shown in Fig. 4.2. When the grid demand is at its highest and the hydrogen production at its lowest between hour 10-15, all three configurations have similar overall efficiency. However, when operating at lower power outputs to the grid, the HTE efficiency has a higher impact on overall efficiency of the entire system. This overall efficiency plot shows that configuration 3 has the highest overall efficiency even though it has a lower Natrium steam cycle thermal efficiency compared to the other configurations. When considering the full system, including hydrogen production, configuration 3 is apparently to be most efficient.

Figures 4.18 and 4.19 show the pump work and total heat input which are used to calculate the thermal efficiency. These two results look very similar across configurations, however, there is one difference in the pump work that stands out. Configuration 2 pump work between hours 5-15 remains constant while the pump work for configuration 1 changes. This is due to the way each is integrated with the hydrogen production. Configuration 1 sees a reduction in pump work due to the changing turbine steam bleed ratios for feedwater

preheating which results in a change in overall mass flow rate of steam. Configuration 2 utilizes hydrogen product to reheat steam which will not change overall flow rate of steam in the system, but will directly reduce heat input needed in the system.

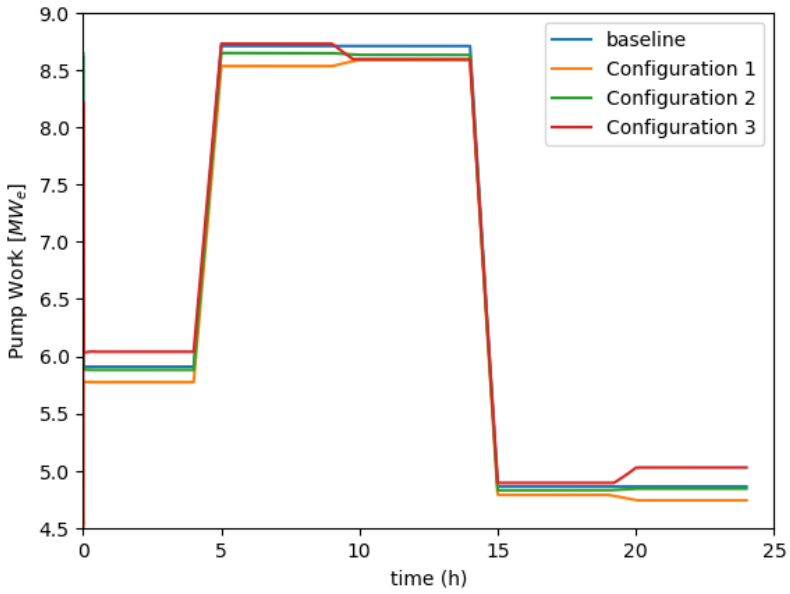

Fig. 4.18: Pump work in BOP for all configurations.

To illustrate molten salt energy storage utilization, Fig. 4.20 shows the rate of change in internal energy of the hot molten salt energy storage tank. Configurations 1 and 2 have a larger rate of molten salt use due to their integration with hydrogen production. A negative dU/dt represents a state of energy boosting and a positive sign is a state of charging.

It is interesting to note that configuration 1 has the larger heat recovery, yet, does not boost steam cycle thermal efficiency as much as configuration 2. Figure 4.21 shows the exergy destruction in the heat exchangers that exchange heat with hydrogen product. Configuration 1 destroys significantly more exergy due to the large temperature difference between the heat exchanger inlet conditions compared to configuration 2.

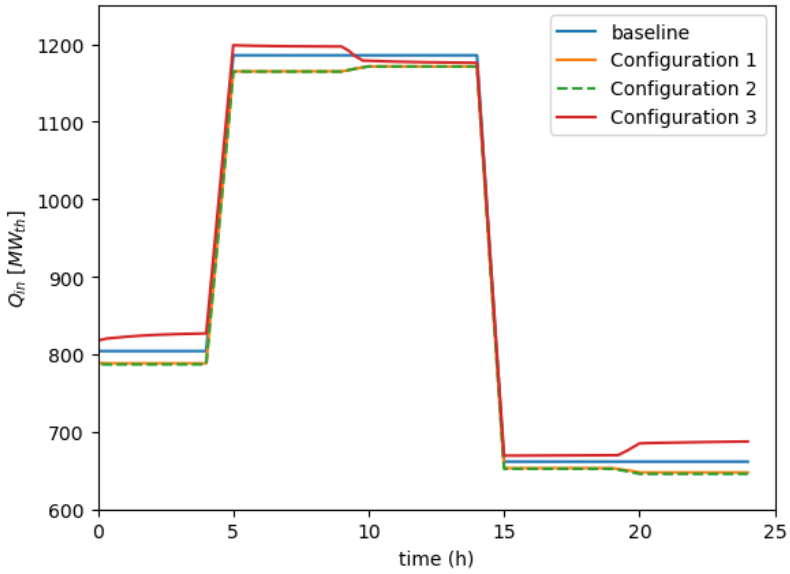

Fig. 4.19: Total heat input in BOP for all configurations.

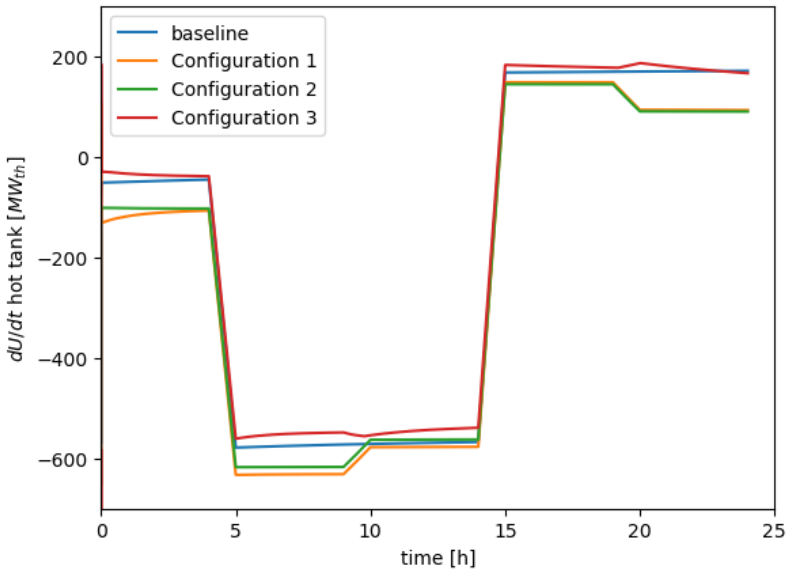

Fig. 4.20: Change of internal energy in the hot molten salt TES tank.

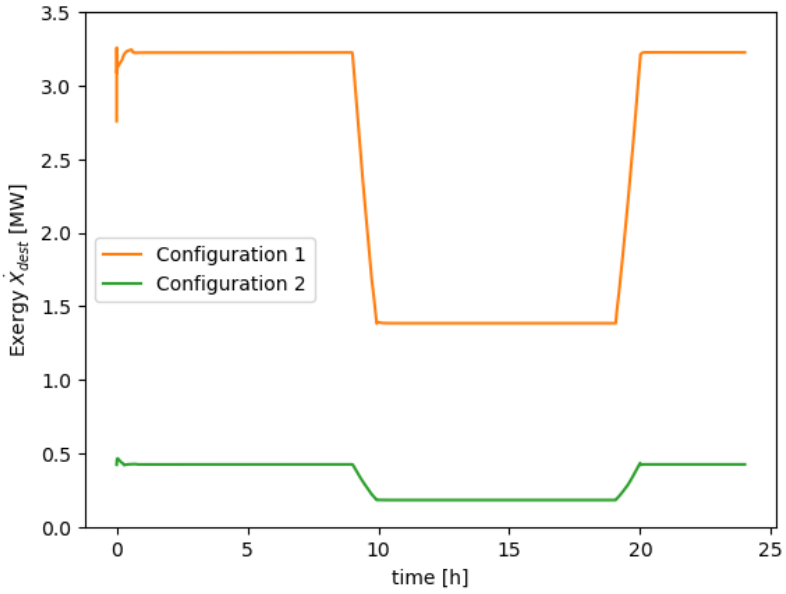

Fig. 4.21: Exergy destruction HTE integration configuration 1 and 2.

4.1.6 Hydrogen Storage Model

This section discusses the results from the hydrogen storage model. As discussed, salt cavern is used as the storage system. To reach the targeted storage pressure, multi-stage compression with intercooling is modeled with the isentropic efficiency of each stage being a constant. hydrogen storage intercooling compression system. In order to minimize power consumption, pressurized hydrogen is cooled back to the inlet temperature. The optimal compression results in each compressor having an equal compression ratio of 2.054. Figure 4.22 shows the temperature vs entropy of the compression cycle. After each compression stage, the fluid is cooled back to 50°C.

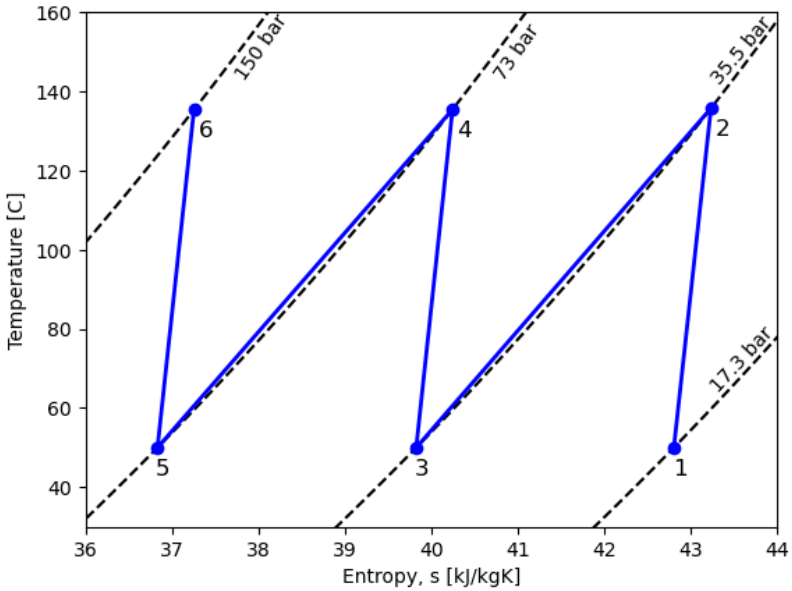

Fig. 4.22: Temperature vs Entropy diagram of multi-stage hydrogen compression.

4.2 HERON Techno-economic Analysis

In this section the results of bi-level optimization and techno economic analysis of the Natrium system with integrated hydrogen production is presented and discussed in details. For each energy market independent system operator (ISO) parametric study results for the baseline Natrium, Natrium with hydrogen production without H2 storage, and Natrium with hydrogen production and storage in underground salt cavity are also shown and discussed to shed some light on various operating modes and designs. The dispatch optimization is also discussed for each market. The sensitivity of hydrogen price is also discussed after presenting results for each individual ISO. Finally, a case study with the optimal dispatch is performed using the dynamic Dymola model for configuration 3 to demonstrate optimal plant operation.

The parametric study in the following sections includes three different systems. First, the baseline system which consists of only the Natrium balance of plant and thermal energy storage (essentially Energy Island). Second, the Natrium system integrated with hydrogen production via HTE. Third, a system like the second one but with salt cavity-based hydrogen

storage. Having the second and third systems intends to demonstrate if adding hydrogen production and storage changes plant operation and economic viability of the system. For the baseline system, the results of sweeping over various BOP and TES capacities are presented. For the systems with hydrogen production, the simulations sweep over HTE production capacity and TES capacity. The hydrogen storage capacity for all three ISO's is 50,000 kg.

4.2.1 CAISO

This section discusses the TEA study for Natrium with hydrogen production in the CAISO (California) energy market. In 2022, the average electricity price was $86,600/GWh. This is the highest average price of all three markets in this work. The max price in 2022 for CAISO was $1.28 million/GWh. This is illustrated in Fig. 4.23 which shows the historical price data that trained the ARMA model. This high average electricity price makes results from the California market different from the Texas and Midwest states results. Figure 4.24 shows the parametric study of the three different systems in CAISO. For all parametric plots in this section, the black points represent capacities evaluated in HERON, the yellow star indicates the capacities with the highest mean NPV, and the contour region is created using linear interpolation between points.

The baseline system parametric results show the optimal system with a BOP size of 0.5 GW_e and TES capacity of 3.5 GWh_{th}. The mean NPV for these capacities is $8.5 million/year. Varying the BOP capacity had a greater affect on the mean npv compared to the TES capacity. The larger electricity generation potential with a larger BOP didn't cover the increase in capital cost of a larger BOP, therefore, the 0.5 GW (500 MW) capacity is the optimal.

The Natrium system coupled with hydrogen production shows different results. For the system with no hydrogen storage the hydrogen demand is equal to the hydrogen capacity, it will operate at fixed output to meet the demand since there is no hydrogen storage. At a price of $4.50, the Natrium system with hydrogen production shows improvement with a mean NPV of $12 million/year. For the case with hydrogen storage the hydrogen market

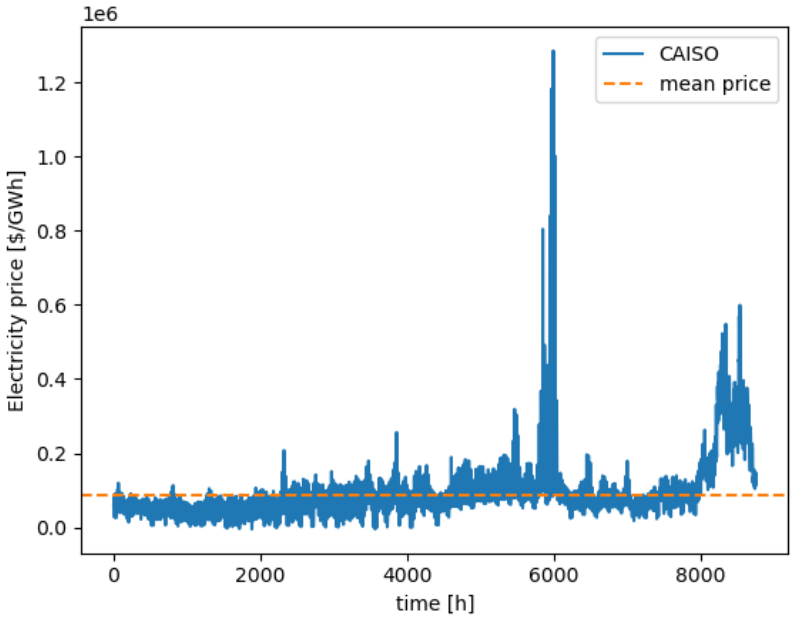

Fig. 4.23: 2022 historical electricity price in CAISO.

demand is set to 3500 kg/h and the hydrogen storage capacity is 50,000 kg of hydrogen. This added flexibility increased the mean NPV up to $20 million/year for the system with hydrogen storage.

The added flexibility of hydrogen storage is illustrated in the dispatch optimization plot as shown in Fig. 4.25. It shows a 72 hour period of system dispatch. It shows the HTE H2 production rate, H2 storage level, electricity dispatched to the grid, TES level, and electricity price. For California, there is significant electricity price flexibility throughout the 3 day period. When the electricity price spikes (see hour 55) the hydrogen production switches off and utilizes hydrogen storage to meet hydrogen market demand. The electricity being sent to the grid quickly ramps up and the thermal energy storage is used to boost power to the full 0.5 GW_e. This same behavior of generating electricity for the grid and switching off hydrogen production occurs multiple times throughout the dispatch period. HTE integration also benefits system economics during price low points as it can use resources to produce and store hydrogen which is more beneficial to the system when

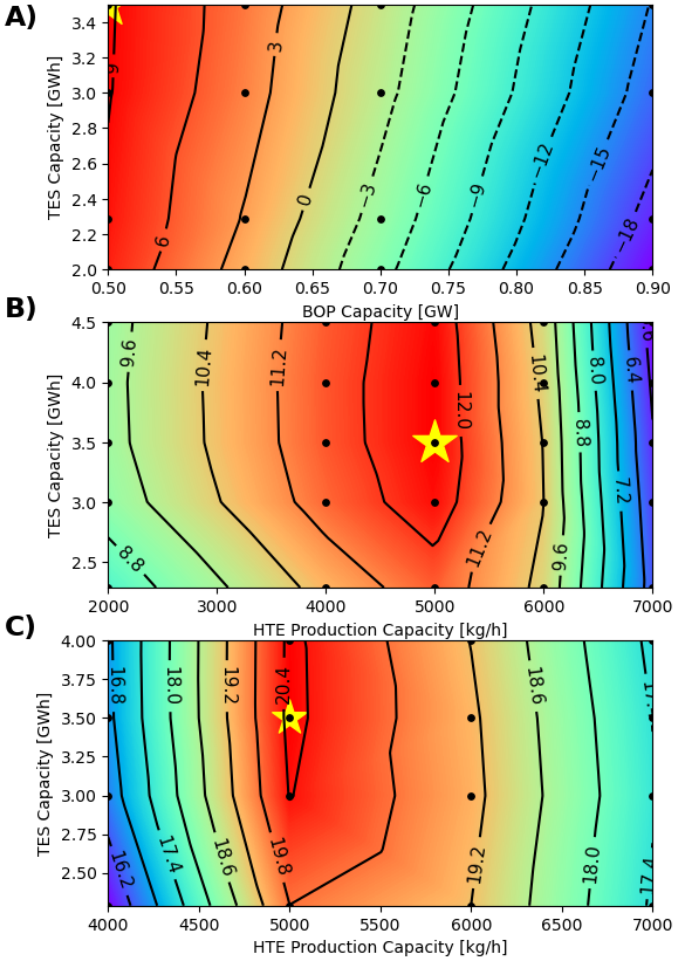

Fig. 4.24: HERON parametric study results CAISO: A) baseline Natrium, B) Natrium with hydrogen production, C) Natrium with hydrogen production and storage (50,000 kg H2).

prices are low. See hours 45-55 leading up to the large price spike, as the system produces hydrogen during the low electricity price.

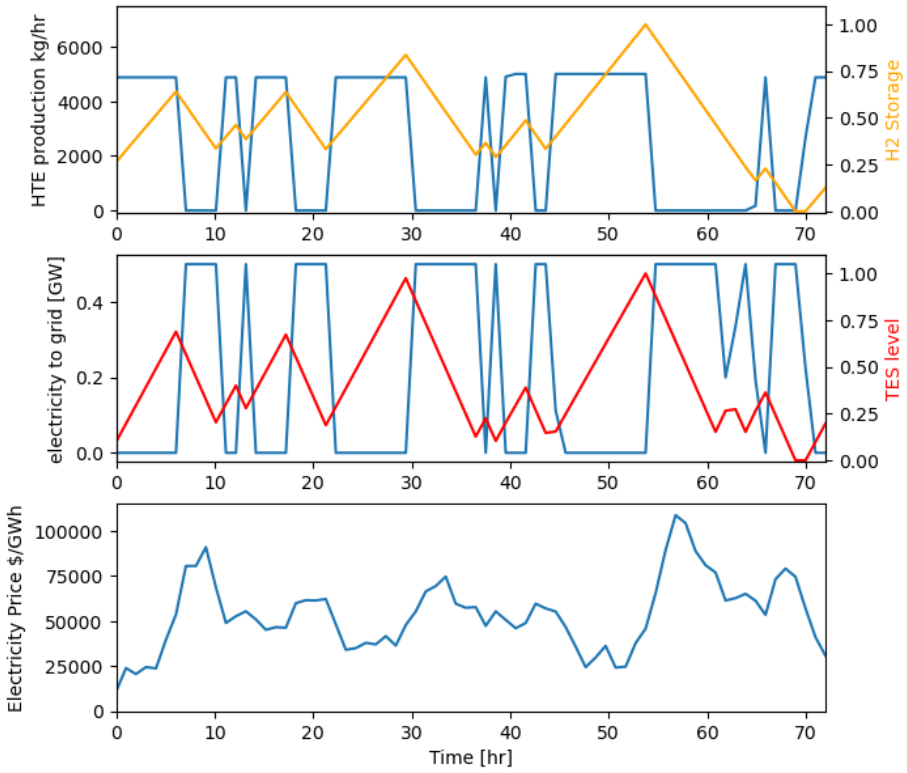

Fig. 4.25: Dispatch optimization of CAISO system for 72 hour period.

4.2.2 ERCOT

This section discusses the TEA study for Natrium with hydrogen production in the ERCOT (Texas) region. In 2022, the average electricity price was $64,300/GWh. This average price is lower than California, however, Texas is known to have extreme price spikes compared to other regions. In 2022, the largest price spike was $2.5 million/GWh with multiple price spikes surpassing $1 million/GWh throughout the year. Figure 4.26 shows the historical price data that trained the ARMA model. Notice how many price spikes are present throughout the year. This section will discuss results from a parametric study which consists of the same systems as were discussed in the CAISO section. Figure 4.27 shows the results from the parametric study for the Texas energy market.

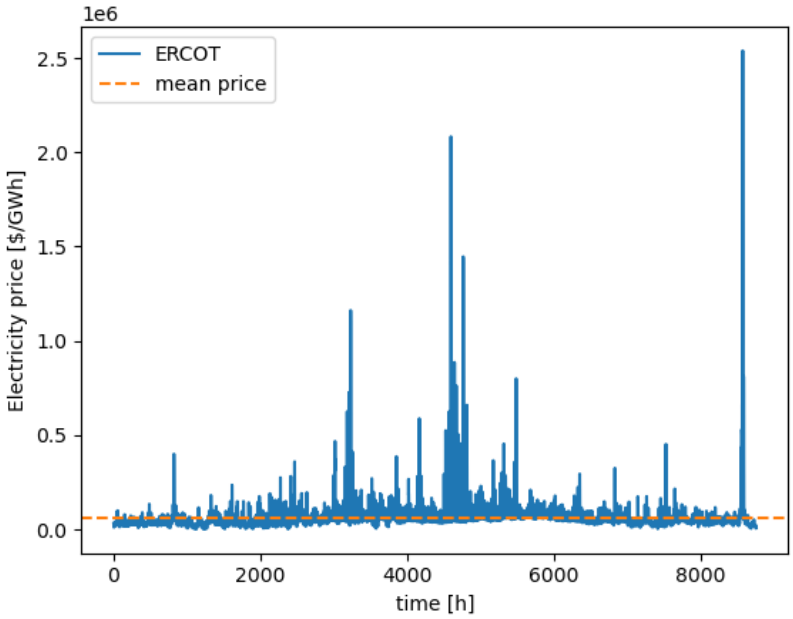

Fig. 4.26: 2022 historical electricity price in ERCOT.

The first thing that stands out in the ERCOT parametric study is the difference in the mean NPV for the baseline system compared to CAISO. The baseline system mean NPV is -$40 million/year with the optimal BOP capacity of 0.5 GW_e and TES capacity of 3.5 GWh_{th}. Even with the same optimal BOP and TES capacities as CAISO, the mean NPV is much lower compared to CAISO due to the different electricity prices in ERCOT.

Introducing hydrogen production at a sell price of $4.50/kg of H2 increases the highest mean NPV to $2.5 million/year with a hydrogen production rate of 7000 kg/h and TES capacity of 2.25 GWh_{th}. For the case with hydrogen storage, the constant hydrogen market demand was set to 6500 kg/h and the hydrogen storage is 50,000 kg. This further improved the mean NPV to $10.4 million/year with a HTE capacity of 7300 kg/h and TES capacity of 2.25 GWh_{th}. Similar to the CAISO results, there is an optimal HTE production capacity for a given hydrogen demand. The HTE capacity is larger than the market demand to allow the system to build up hydrogen in storage. When there is a price spike in electricity price the hydrogen storage can be used to meet market demand while the Natrium ramps up to maximum electricity production. Figure 4.28 shows the optimal dispatch of electricity and

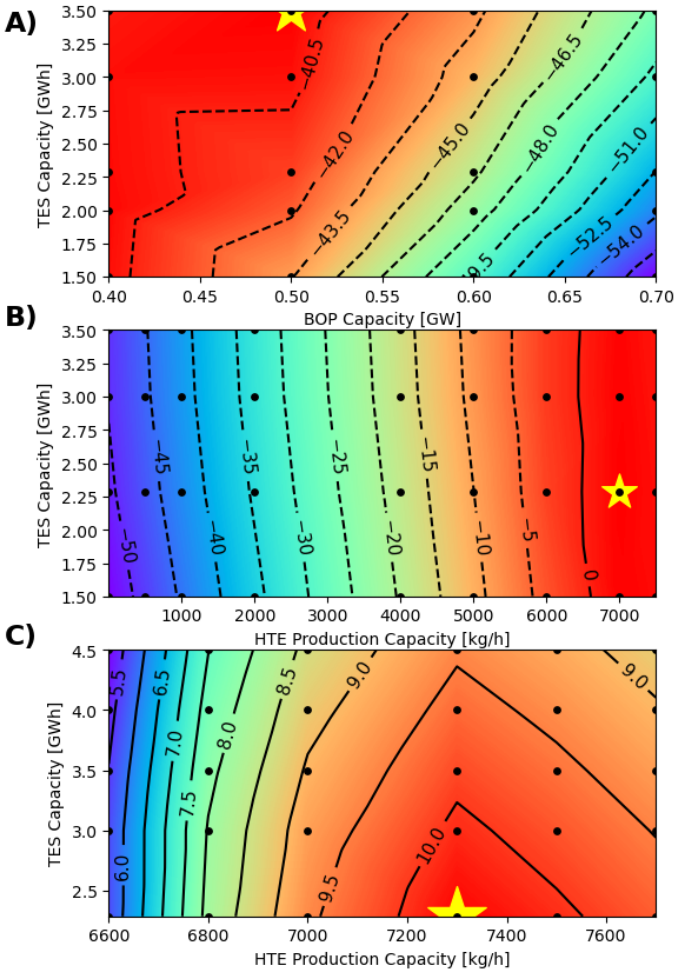

Fig. 4.27: HERON parametric study results Texas: A) baseline Natrium, B) Natrium with hydrogen production, C) Natrium with hydrogen production and storage (50,000 kg H2).

hydrogen over a 72 hour period. It is similar to the CAISO results, however, there are fewer time periods with large electricity price spikes.

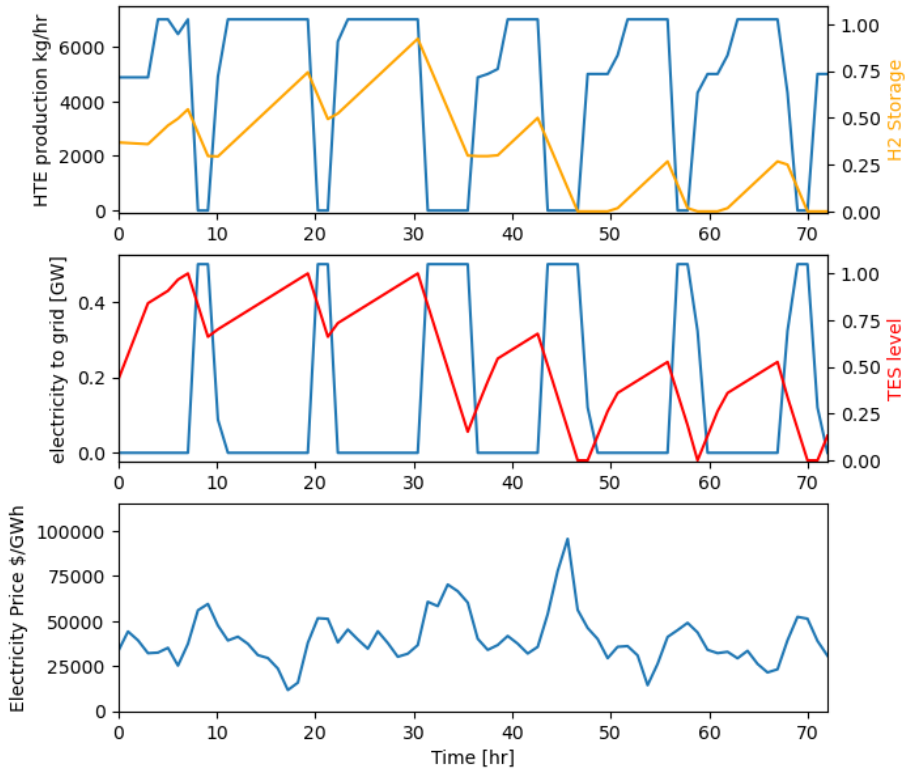

Fig. 4.28: Dispatch optimization of ERCOT system for 72 hour period.

4.2.3 MISO

Finally, this section will discuss the TEA study for Natrium with on-site hydrogen production in the MISO (Midwest states) region. The MISO market consists of the following states: North Dakota, Minnesota, Iowa, Wisconsin, Michigan, Illinois, Indiana, Arkansas, Mississippi, Louisiana, and portions of states in the surrounding area. In 2022, the average price of electricity was $57,000/GWh which is the lowest of all three ISOs. This difference can be seen in Fig. 4.29 which shows the 2022 historical electricity price in MISO. Additionally, the maximum price seen in 2022 was $260,000/GWh. This region sees smaller price spikes compared to the other two regions in this study. Figure 4.30 shows the results from the parametric study.

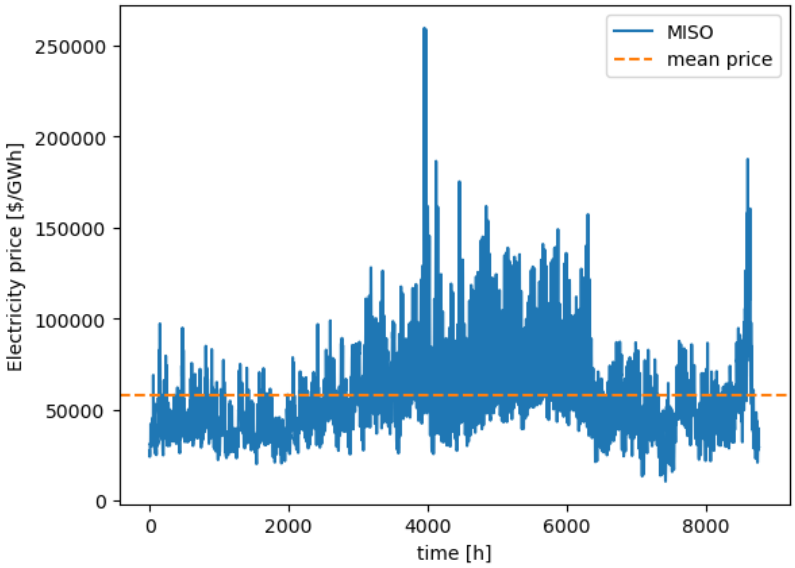

Fig. 4.29: 2022 historical electricity price in MISO.

Similar to ERCOT, the baseline Natrium system results show a mean NPV of -$51 million/year with a BOP capacity of 0.4 GW_e and TES capacity of 2 GWh_{th}. Adding hydrogen to the system does increase the mean NPV to -$5 million/year with an HTE capacity of 7000 kg/h and TES of 1.5 GWh_{th}. The results of adding 50,000 kg of hydrogen storage with a hydrogen market demand of 6500 kg/h did not improve the mean NPV for this market. The primary purpose of adding hydrogen storage is to allow the Natrium system to switch between hydrogen production and electricity generation. With electricity prices being the lowest and least volatile of all three ISO's, the system does not switch to electricity generation as often compared to the previous two locations. This results in the added hydrogen storage not having a large effect on mean NPV calculations. Figure 4.31 illustrates how this market has less dynamic operation among its subsystems. Additionally, the dispatch plots for MISO show how the hydrogen storage is never filled during this 3 day period. This further illustrates that hydrogen storage is not essential for MISO compared to the other markets.

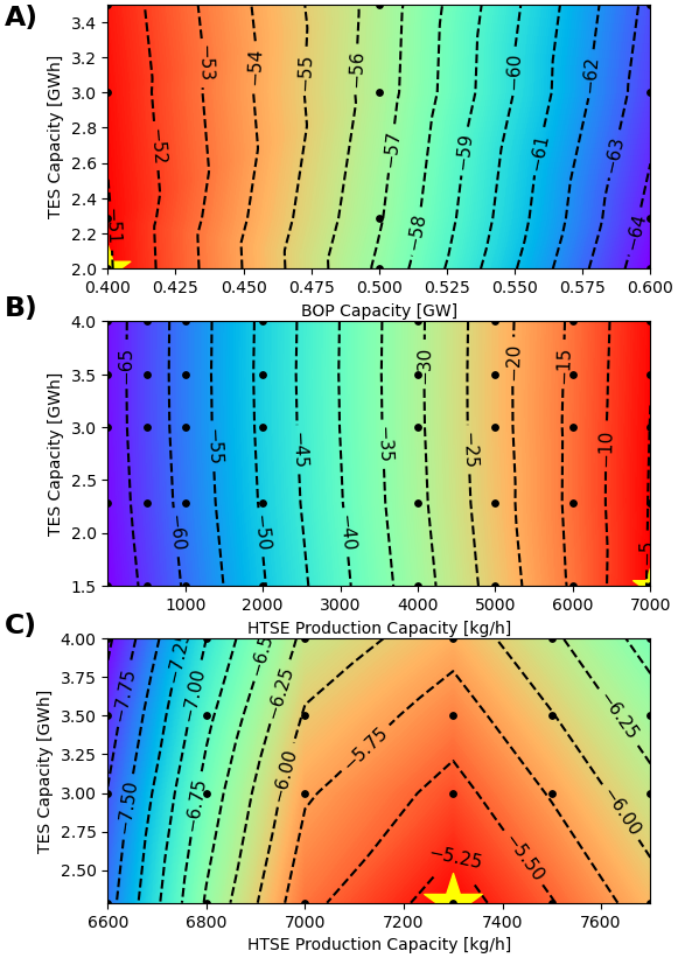

Fig. 4.30: HERON parametric study results MISO: A) baseline Natrium, B) Natrium with hydrogen production, C) Natrium with hydrogen production and storage (50,000 kg H2).

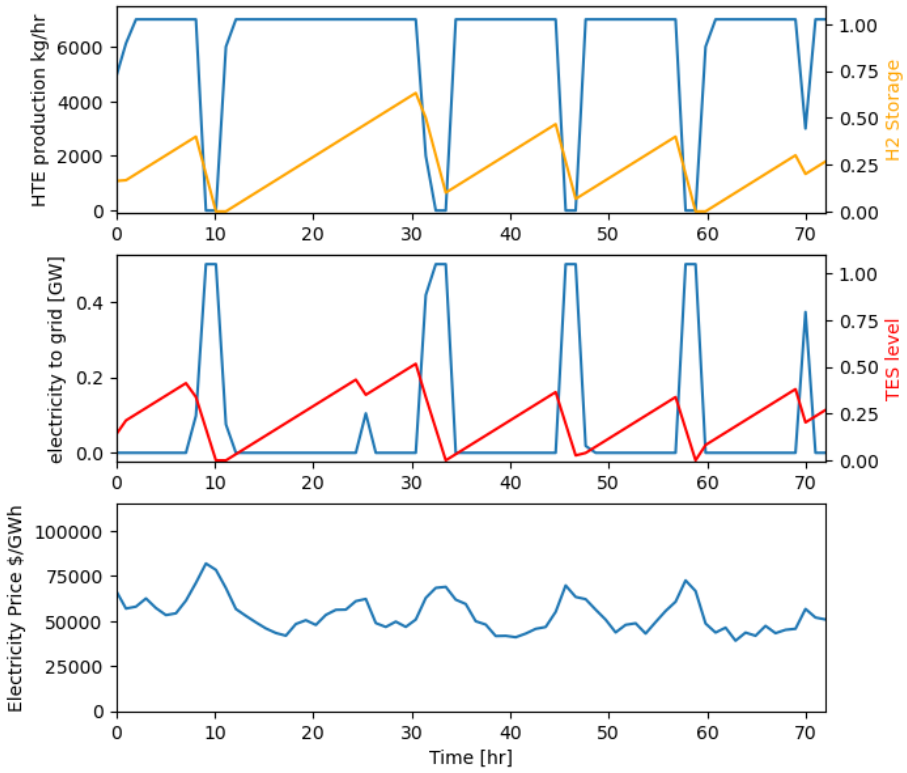

Fig. 4.31: Dispatch optimization of MISO system for 72 hour period.

4.2.4 Discussion of TEA Results

The TEA analysis of the Natrium system revealed that hydrogen production can increase plant flexibility which in turn can increase the mean NPV of the system. However, the parametric study plots do not show the distribution of NPV's calculated during HERON parametric sweep with its ability to simulate many electricity price profiles using synthetic time series. Figure 4.32 shows a sensitivity study on how the market price of hydrogen affects the mean NPV of the Natrium system with hydrogen production and storage. Each point used 510 synthetic histories to calculate the mean NPV. This plot also includes the upper and lower bounds with 95% confidence for all data presented in the plot. Table 4.1 shows the main component capacities used in calculating results in Fig. 4.32. The baseline values refer to Natrium system with no hydrogen integration.

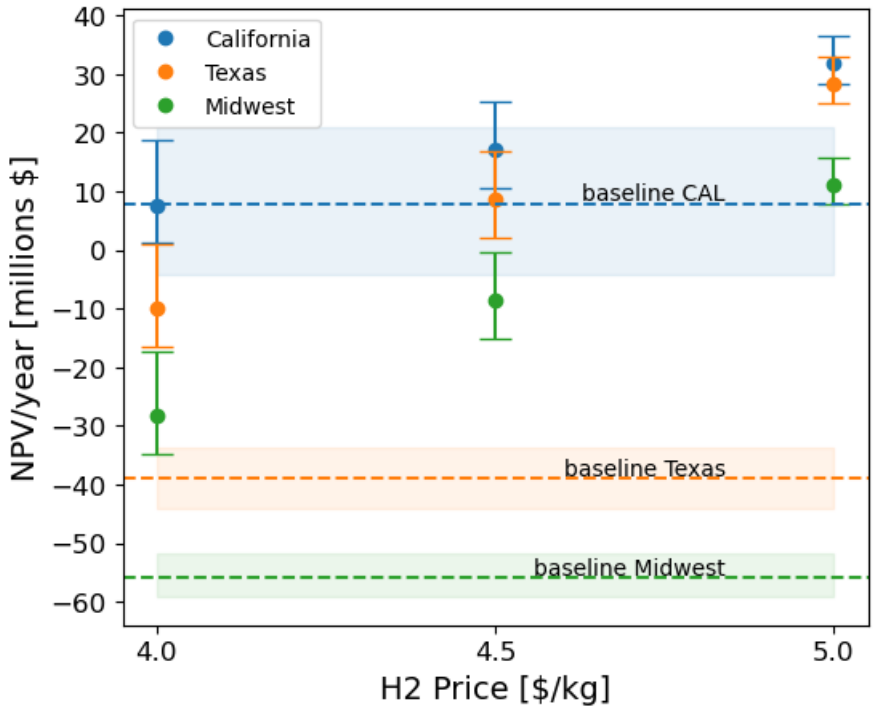

Fig. 4.32: Sensitivity analysis of hydrogen price and baseline Natrium.

Table 4.1: System capacities for H2 price sensitivity analysis. High, Med, and Low refer to $5.00/kg, $4.50/kg, and $4.00/kg hydrogen market prices respectively.

	TES $[GWh_{th}]$	**HTE** $[\frac{kg}{h}]$	**H2 Market** $[\frac{kg}{h}]$	**H2 Storage** $[kg]$
CAISO High	2.288	7000	5500	40000
CAISO Med	3.5	5000	3500	35000
CAISO Low	3.5	4500	2500	40000
ERCOT High	2.288	7000	6500	40000
ERCOT Med	2.288	7000	6500	40000
ERCOT Low	2.288	7000	5500	40000
MISO High	2.288	7000	6500	30000
MISO Med	2.288	7000	6500	30000
MISO Low	2.288	7000	6500	30000

As illustrated in the Fig. 4.32, as the hydrogen price increases, the 95% limits begin to shrink. This is because at higher hydrogen prices, especially in the California market, the size of the HTE capacity increases, therefore an increasing portion of plant revenue comes from the constant hydrogen market rather than the volatile electricity market. The higher

uncertainty (broader shaded band) of the CAISO baseline occurs due to the volatile nature of the electricity price in that region. Another characteristic of the distribution of NPV can be seen at the low H2 market price, the 95% limits are not centered at the mean (slightly skewed). This is due to the nature of the distribution of electricity prices in each market. The price spikes are much larger than the price dips, therefore the uncertainty in the mean NPV will have a similar skew.

4.3 Case Study - Dispatch Simulation

This section presents a case study of an optimized CAISO dispatch simulated using Dymola configuration 3. The dispatch shown in Fig. 4.33 includes the net electricity sent to the grid, hydrogen production rate, TES level, hydrogen storage level, and electricity prices.

These dispatch plots show the optimal dispatch of configuration 3 based on the electricity price. The system tends to operate in two conditions: max hydrogen production or maximum net electricity to the grid. During periods of lower electricity prices the system stores hydrogen and energy in the TES in order to boost electricity production and use hydrogen storage during peak electricity prices. This simulation validates the dispatch from the HERON optimization that the input profiles (W_{net} and H2 Production) work for configuration 3.

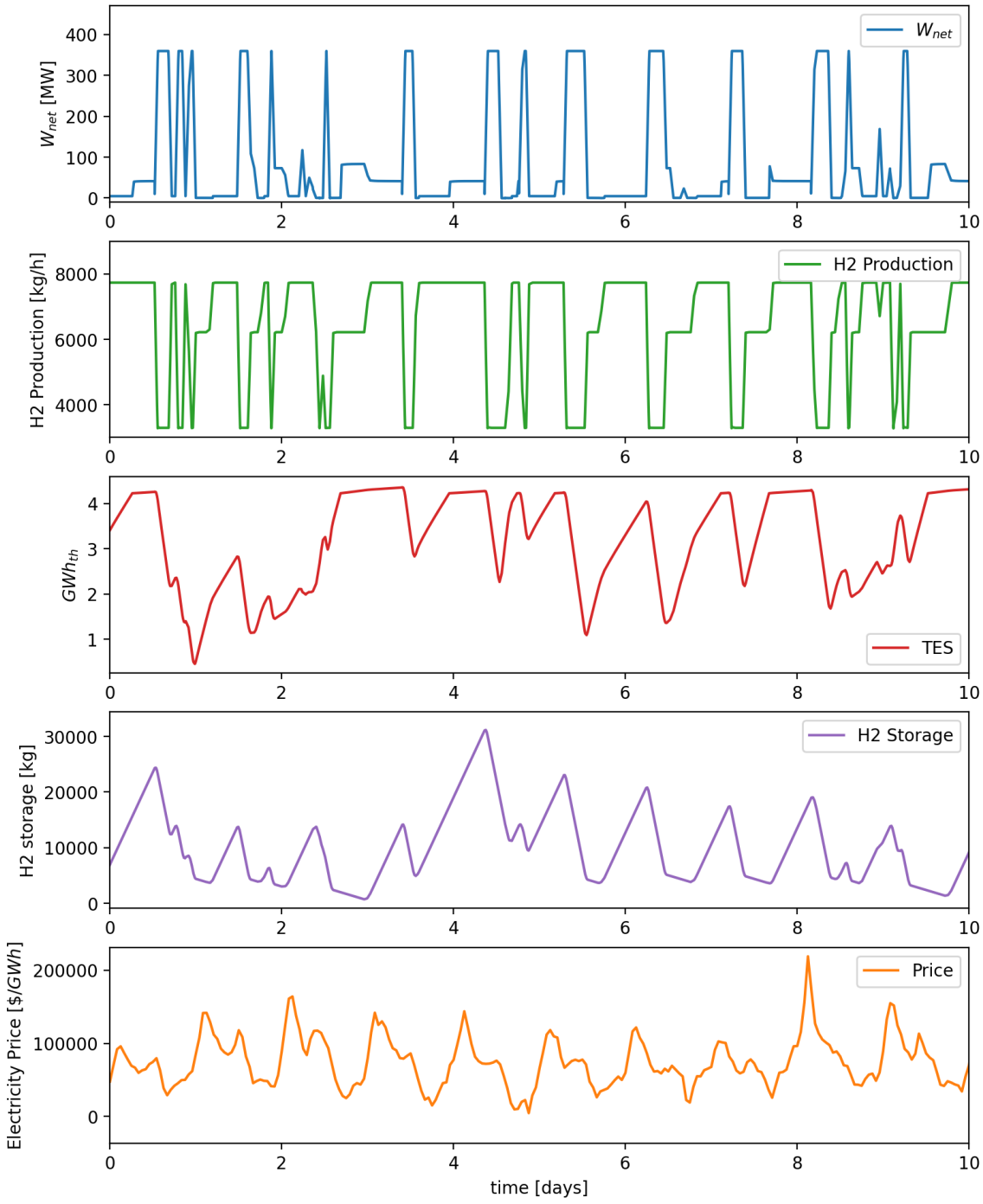

Fig. 4.33: 10 day simulation results from configuration 3 dispatch validation. Net power generation, H2 production, TES level, H2 storage level, and electricity price.

CHAPTER 5

CONCLUSION

This thesis provided an analysis of integrating hydrogen production via high temperature steam electrolysis with the Natrium advanced reactor design by TerraPower and GE Hitachi. The Natrium design is an advanced reactor technology which utilizes a sodium fast reactor and molten salt thermal energy storage. The analysis included a literature review on nuclear integrated energy system modeling, GEN III reactor hydrogen co-generation, high temperature steam electrolysis, and hydrogen storage technologies.

The results analyzed three different configurations that thermally integrate the Natrium Energy Island to the HTE system. Configurations 1 and 2 integrated Energy Island through molten salt TES tanks and recuperated energy from the hydrogen product. These models show that both of these configurations can boost steam cycle thermal efficiency up to 1%. Configuration 3 integrated Energy Island by utilizing low grade steam from the steam cycle as feedstock for the HTE process. While this configuration does not improve thermal efficiency of the steam cycle, the HTE efficiency is greater than the other two configurations and the overall system efficiency is improved. In addition, configuration 3 is less complex compared to the other configuration while having an apparent improvement in overall system efficiency.

The techno-economic analysis revealed that for ERCOT and CAISO hydrogen production *and* storage increases plant flexibility and improves plant economics. Hydrogen production increases economics for MISO, however, hydrogen storage does not show any additional benefits for that energy market. Comparing economic results to the baseline Natrium system, adding hydrogen production improved NPV for MISO and ERCOT. Hydrogen production improved NPV in CAISO market when the hydrogen price is $5/kg or greater. Hydrogen production can provide economic stability for the Nuclear plant due to its constant price and production rate compared to the volatile electricity market.

Future recommended work include some of the following possibilities:

- Increase size of HERON system to include solar power, wind power, and specified energy demand.
- Add complexity to salt cavity storage dymola model to include pressure changes inside cavity during different charge levels.
- Model heat exchangers to include thermal mass for transient modeling with smaller time constants.
- Include distribution and process modeling for hydrogen product (ammonia production, chemical process, etc)

REFERENCES

[1] "U.S. energy consumption increases between 0% and 15% by 2050," *U.S. Energy Information Administration*, April 2023, https://www.eia.gov/todayinenergy/detail.php?id=56040.

[2] "Frequently Asked Questions (FAQs) - U.S. Energy Information Administration (EIA)," *U.S. Energy Information Administration*, April 2023, https://www.eia.gov/todayinenergy/detail.php?id=56040.

[3] "Hydrogen Production: Natural Gas Reforming," *Office of Energy Efficiency & Renewable Energy*, https://www.energy.gov/eere/fuelcells/hydrogen-production-natural-gas-reforming.

[4] "Hydrogen Storage," *Office of Energy Efficiency & Renewable Energy*, https://www.energy.gov/eere/fuelcells/hydrogen-storage.

[5] FitzGerald, D. M., Fenster, M. S., Argow, B. A., and Buynevich, I. V., "Coastal Impacts Due to Sea-Level Rise," *Annual Review of Earth and Planetary Sciences*, Vol. 36, No. 1, 2008, pp. 601–647, _eprint: https://doi.org/10.1146/annurev.earth.35.031306.140139.

[6] Brooks, H. E., "Severe thunderstorms and climate change," *Atmospheric Research*, Vol. 123, April 2013, pp. 129–138.

[7] Mancosu, N., Snyder, R. L., Kyriakakis, G., and Spano, D., "Water Scarcity and Future Challenges for Food Production," *Water*, Vol. 7, No. 3, March 2015, pp. 975–992, Number: 3 Publisher: Multidisciplinary Digital Publishing Institute.

[8] "Sources of Greenhouse Gas Emissions | Greenhouse Gas (GHG) Emissions," *U.S. Enviornmental Protection Agency*, https://climatechange.chicago.gov/ghgemissions/sources-greenhouse-gas-emissions.

[9] Kerry, J., "The Long-Term Strategy of the United States, Pathways to Net-Zero Greenhouse Gas Emissions by 2050," .

[10] Park, W.-J., Song, K.-B., and Park, J.-W., "Impact of Electric Vehicle Penetration-Based Charging Demand on Load Profile," *Journal of Electrical Engineering and Technology*, Vol. 8, March 2013.

[11] Branker, K., Pathak, M., and Pearce, J., "A review of solar photovoltaic levelized cost of electricity," *Renewable and Sustainable Energy Reviews*, Vol. 15, No. 9, Dec. 2011, pp. 4470–4482, Number: 9.

[12] "Energy Flow Charts: Charting the Complex Relationships among Energy, Water, and Carbon," *Lawrence Livermore National Laboratory*, 2021, https://flowcharts.llnl.gov/.

[13] OECD, *Technical and Economic Aspects of Load Following with Nuclear Power Plants*, Nuclear Development, OECD, Dec. 2021.

[14] Owen, A. D., "The economic viability of nuclear power in a fossil-fuel-rich country: Australia," *Energy Policy*, Vol. 39, No. 3, March 2011, pp. 1305–1311.

[15] NEA, "Nuclear Energy Today: Second Edition," *OECD Publishing*, 2012, https://www.oecd-nea.org/jcms/pl_14560/nuclear-energy-today-second-edition?details=true.

[16] Locatelli, G., Boarin, S., Fiordaliso, A., and Ricotti, M. E., "Load following of Small Modular Reactors (SMR) by cogeneration of hydrogen: A techno-economic analysis," *Energy*, Vol. 148, April 2018, pp. 494–505, Publisher: Pergamon.

[17] Forsberg, C., "Hybrid systems to address seasonal mismatches between electricity production and demand in nuclear renewable electrical grids," *Energy Policy*, Vol. 62, Nov. 2013, pp. 333–341.

[18] Khamis, I., Koshy, T., and Kavvadias, K. C., "Opportunity for Cogeneration in Nuclear Power Plants," *Advances in Nano, Biomechanics, Robotics, and Energy Research*, Seoul, Korea, 2013.

[19] Hills, S., Dana, S., and Wang, H., "Dynamic modeling and simulation of nuclear hybrid energy systems using freeze desalination and reverse osmosis for clean water production," *Energy Conversion and Management*, Vol. 247, Nov. 2021, pp. 114724.

[20] Bryan, J., Meek, A., Dana, S., Islam Sakir, M. S., and Wang, H., "Modeling and design optimization of carbon-free hybrid energy systems with thermal and hydrogen storage," *International Journal of Hydrogen Energy*, March 2023.

[21] Frick, K., Talbot, P., Wendt, D., Boardman, R., Rabiti, C., Bragg-Sitton, S., Ruth, M., Levie, D., Frew, B., Elgowainy, A., and Hawkins, T., "Evaluation of Hydrogen Production Feasibility for a Light Water Reactor in the Midwest," Tech. Rep. INL/EXT-19-55395-Rev000, 1569271, Sept. 2019.

[22] Wodrich, L., Lee, A. J. H., Kozlowski, T., and Brooks, C. S., "Modeling of an Energy-Diverse Embedded Grid for Microreactor Integration," *Nuclear Technology*, Vol. 209, No. 6, June 2023, pp. 809–834.

[23] Binder, W., Paredis, C., and Garcia, H., "Hybrid Energy System Modeling in Modelica," *the 10th International Modelica Conference*, Lund, Sweden, March 2014, pp. 979–988.

[24] Shin, Y., Park, W., Chang, J., and Park, J., "Evaluation of the high temperature electrolysis of steam to produce hydrogen," *International Journal of Hydrogen Energy*, Vol. 32, No. 10-11, July 2007, pp. 1486–1491.

[25] Ivy, J., "Summary of Electrolytic Hydrogen Production: Milestone Completion Report," *National Renewable Energy Laboratory*, 2004.

[26] Yildiz, B. and Kazimi, M., "Efficiency of hydrogen production systems using alternative nuclear energy technologies," *International Journal of Hydrogen Energy*, Vol. 31, No. 1, Jan. 2006, pp. 77–92.

[27] Mingyi, L., Bo, Y., Jingming, X., and Jing, C., "Thermodynamic analysis of the efficiency of high-temperature steam electrolysis system for hydrogen production," *Journal of Power Sources*, Vol. 177, No. 2, March 2008, pp. 493–499.

[28] Gangu, K. K., Maddila, S., and Jonnalagadda, S. B., "The pioneering role of metal–organic framework-5 in ever-growing contemporary applications – a review," *RSC Advances*, Vol. 12, No. 22, 2022, pp. 14282–14298.

[29] Ozarslan, A., "Large-scale hydrogen energy storage in salt caverns," *International Journal of Hydrogen Energy*, Vol. 37, No. 19, Oct. 2012, pp. 14265–14277.

[30] Kruck, O., Crotogino, F., Prelicz, R., and Rudolph, T., "Overview on all Known Underground Storage Technologies for Hydrogen," *HyUnder*, 2013, Technical Report.

[31] Ho, A., Hill, D., Hedengren, J., and Powell, K. M., "A nuclear-hydrogen hybrid energy system with large-scale storage: A study in optimal dispatch and economic performance in a real-world market," *Journal of Energy Storage*, Vol. 51, July 2022, pp. 104510.

[32] Yang, C., Wang, T., Li, Y., Yang, H., Li, J., Qu, D., Xu, B., Yang, Y., and Daemen, J., "Feasibility analysis of using abandoned salt caverns for large-scale underground energy storage in China," *Applied Energy*, Vol. 137, Jan. 2015, pp. 467–481.

[33] "The Basics of Underground Natural Gas Storage," *U.S. Energy Information Administration*, https://www.eia.gov/naturalgas/storage/basics/.

[34] "Advanced Clean Energy Storage," *Loan Programs Office*, https://www.energy.gov/lpo/advanced-clean-energy-storage.

[35] "Aiming for Clean Power Generation with 100% Hydrogen," *Mitsubishi Power*, https://power.mhi.com/case/america_utah.

[36] Wang, Y., Kowal, J., Leuthold, M., and Sauer, D. U., "Storage System of Renewable Energy Generated Hydrogen for Chemical Industry," *Energy Procedia*, Vol. 29, 2012, pp. 657–667.

[37] Ma, N., Zhao, W., Wang, W., Li, X., and Zhou, H., "Large scale of green hydrogen storage: Opportunities and challenges," *International Journal of Hydrogen Energy*, Sept. 2023.

[38] Tarhan, C. and Çil, M. A., "A study on hydrogen, the clean energy of the future: Hydrogen storage methods," *Journal of Energy Storage*, Vol. 40, Aug. 2021, pp. 102676.

[39] Elsheikh, A., Widl, E., and Palensky, P., "Simulating complex energy systems with Modelica: A primary evaluation," *2012 6th IEEE International Conference on Digital Ecosystems and Technologies (DEST)*, June 2012, pp. 1–6, ISSN: 2150-4946.

[40] "Dymola," *Dassault Systemes*, https://www.3ds.com/products-services/catia/products/dymola/.

[41] Reddy Prasad, D., Senthilkumar, R., Lakshmanarao, G., Krishnan, S., Naveen Prasad, B., 1 Petroleum and Chemical Engineering Programme area, Faculty of Engineering, Universiti Teknologi Brunei, Gadong, Brunei Darussalam, 2 Department of Engineering, College of Applied Sciences, Sohar, Sultanate of Oman, and 3 Sathyabama Institute of Science and Technology, Chennai, India, "A critical review on thermal energy storage materials and systems for solar applications," *AIMS Energy*, Vol. 7, No. 4, 2019, pp. 507–526.

[42] Wu, Y.-t., Li, Y., Lu, Y.-w., Wang, H.-f., and Ma, C.-f., "Novel low melting point binary nitrates for thermal energy storage applications," *Solar Energy Materials and Solar Cells*, Vol. 164, May 2017, pp. 114–121.

[43] Zavoico, A. B., "Solar Power Tower Design Basis Document, Revision 0," Tech. Rep. SAND2001-2100, 786629, July 2001.

[44] Meek, A. S., Dana, S. J., Bryan, J., Basnet, M., and Wang, H., "Steady State Modeling of a Regenerative Rankine Cycle for the Natrium System," *ASME 2023 17th International Conference on Energy Sustainability*, American Society of Mechanical Engineers, Washington, DC, USA, July 2023, p. V001T08A005.

[45] Greenwood, M., Harrison, T., Qualls, L., Fugate, D., Hale, R., and Cetiner, S., "TRANSFORM - TRANsient Simulation Framework of Reconfigurable Models," *Oak Ridge National Laboratory*, 2017.

[46] Kim, J. S., Bragg-Sitton, S. M., and Boardman, R. D., "Status Report on the High-Temperature Steam Electrolysis Plant Model Developed in the Modelica Framework (FY17)," Tech. Rep. INL/EXT–17-43056, 1408745, Aug. 2017.

[47] Stoots, C. M., O'Brien, J. E., McKellar, M. G., Hawkes, G. L., and Herring, S. J., "Engineering Process Model for High-Temperature Electrolysis System Performance Evaluation," 2005.

[48] Jarungthammachote, S., "Optimal interstage pressures of multistage compression with intercooling processes," *Thermal Science and Engineering Progress*, Vol. 29, March 2022, pp. 101202.

[49] Talbot, P., McDowell, D., Richards, J., Cogliati, J., Alfonsi, A., Rabiti, C., Boardman, R., Bernhoft, S., La Chesnaye, F., Ela, E., Hytowitz, R., Kerr, C., Taber, J., Tuohy, A., and Ziebell, D., "Evaluation of Hybrid FPOG Applications in Regulated and Deregulated Markets Using HERON," Tech. Rep. INL/EXT–20-60968, 1755894, Dec. 2020.

[50] Talbot, P. W., Rabiti, C., Alfonsi, A., Krome, C., Kunz, M. R., Epiney, A., Wang, C., and Mandelli, D., "Correlated synthetic time series generation for energy system simulations using Fourier and ARMA signal processing," *International Journal of Energy Research*, Vol. 44, No. 10, 2020, pp. 8144–8155, _eprint: https://onlinelibrary.wiley.com/doi/pdf/10.1002/er.5115.

[51] Epiney, A. S., Talbot, P., Wang, C., Alfonsi, A., and Worsham, E., "Tool for Economic Analysis (TEAL) User Manual," *Idaho National Laboratory*, April 2024.

[52] Hansen, J., Jenson, W., Wrobel, A., Stauff, N., Biegel, K., Kim, T., Belles, R., and Omitaomu, F., "Investigating Benefits and Challenges of Converting Retiring Coal Plants into Nuclear Plants," Tech. Rep. INL/RPT-22-67964-Rev000, 1886660, Sept. 2022.

[53] Hill, D., Martin, A., Martin-Nelson, N., Granger, C., Memmott, M., Powell, K., and Hedengren, J., "Techno-economic sensitivity analysis for combined design and operation of a small modular reactor hybrid energy system," *International Journal of Thermofluids*, Vol. 16, Nov. 2022, pp. 100191.

[54] Mikkelson, D., Frick, K., Bragg-Sitton, S., and Doster, J. M., "Phenomenon Identification and Ranking Table Development for Future Application Figure-of-Merit Studies on Thermal Energy Storage Integrations with Light Water Reactors," *Nuclear Technology*, Vol. 208, No. 3, March 2022, pp. 437–454.

[55] Wendt, D., Knighton, L., and Boardman, R., "High Temperature Steam Electrolysis Process Performance and Cost Estimates," Tech. Rep. INL/RPT-22-66117-Rev000, 1867883, March 2022.

[56] Papadias, D. D. and Ahluwalia, R. K., "Bulk storage of hydrogen," *International Journal of Hydrogen Energy*, Vol. 46, No. 70, Oct. 2021, pp. 34527–34541.

APPENDIX

HERON INPUT XML FILE

The HERON input file generates an outer.xml file which serves as input to RAVEN. The input file in this appendix contains all components: nuclear power plant line 45 (NPP), thermal energy storage line 218 (TES), balance of plant 83 (BOP), grid line 176, high temperature electrolysis line 132 (HTE), H2 storage line 250 and H2 market line 197. For simulations without HTE components, those sections of the input file are removed. The file below is for the CAISO electricity market with a medium H2 price of $4.50.

~\projects\etri1\1caiso\sweep_caiso_with_h2_storage_med.xml

```
<HERON>
  <Case name="CAISO_with_H2_storage_SWEEP_med">
    <mode>sweep</mode>
    <!-- <debug>
      <inner_samples>1</inner_samples>
      <macro_steps>1</macro_steps>
      <dispatch_plot>True</dispatch_plot>
    </debug> -->
    <num_arma_samples>30</num_arma_samples>
    <parallel>
      <outer>2</outer>
      <inner>5</inner>
    </parallel>
    <time_discretization>
      <time_variable>HOUR</time_variable>
      <year_variable>YEAR</year_variable>
      <end_time>729</end_time>
      <num_steps>730</num_steps>  <!-- segments of about 1 month -->
    </time_discretization>
    <economics>
      <ProjectTime>1</ProjectTime>
      <DiscountRate>0.08</DiscountRate>
      <tax>0.25</tax>
      <inflation>0.025</inflation>
      <verbosity>50</verbosity>
    </economics>
    <dispatcher>
      <pyomo>
        <rolling_window_length>168</rolling_window_length>  <!-- 1 week -->
      </pyomo>
    </dispatcher>
    <optimization_settings>rav
      <opt_metric>NPV</opt_metric>
      <stats_metric>expectedValue</stats_metric>
      <type>max</type>
      <persistence>2</persistence>
      <convergence>
        <stepSize>1e-4</stepSize>
      </convergence>
    </optimization_settings>
  </Case>

  <Components>
    <!--PRODUCING COMPONENTS-->
    <Component name="NPP">
```

```
      <produces resource="heat" dispatch="fixed">
        <capacity resource="heat">
          <fixed_value>0.8625</fixed_value>  <!-- Always fixed! -->
        </capacity>
      </produces>
      <economics>
        <!-- <lifetime>60</lifetime> -->
        <lifetime>1</lifetime>
        <CashFlow name="capex" type="one-time" taxable="True" inflation="none" mult_target="False">  <!-- OCC from NPP construction, C2N#3 (Hansen 2022, Coal to Nuclear report) -->
          <driver>
            <variable>NPP_capacity</variable>
          </driver>
          <reference_price> <!-- [-1140e6, -1520e6] at 40% BOP eff -->
            <fixed_value>-113.117e6</fixed_value>  <!-- Scaled for 1 year -->
            <!-- <fixed_value>-1330e6</fixed_value> -->  <!-- Value for 60-year lifetime -->
          </reference_price>
          <!-- <depreciate>15</depreciate> -->
        </CashFlow>
        <CashFlow name="FOM" type="repeating" period="year" taxable="True" inflation="none" mult_target="False">  <!-- FOM from C2N#3 (Hansen 2022, Coal to Nuclear report) -->
          <driver>
            <variable>NPP_capacity</variable>
          </driver>
          <reference_price> <!-- [-41.6e6, -48.0e6] at 40% BOP eff -->
            <fixed_value>-44.8e6</fixed_value>
          </reference_price>
        </CashFlow>
        <CashFlow name="VOM" type="repeating" taxable="True" inflation="none" mult_target="False">  <!-- VOM + Fuel Cost from C2N#3 (Hansen 2022, Coal to Nuclear report) -->
          <driver>
            <activity>heat</activity>
          </driver>
          <reference_price> <!-- [-6.6044e3, -8.2574e3] with 40% BOP eff -->
            <fixed_value>-7.43e3</fixed_value>
          </reference_price>
        </CashFlow>
      </economics>
    </Component>

    <Component name="BOP">
      <produces resource="electricity" dispatch="independent">
        <consumes>heat</consumes>
        <capacity resource="electricity">
          <!-- 500 MW is the Natrium design point -->
```

```
          <fixed_value debug_value='0.5'>0.5</fixed_value> <!--capacity bounds 400 and 900 MWe-->
        </capacity>
        <minimum resource="electricity">
          <fixed_value>0.2</fixed_value>
        </minimum>
        <transfer>
          <linear>
            <rate resource="heat">-1</rate>
            <rate resource="electricity">0.4</rate>
          </linear>
        </transfer>
      </produces>
      <economics>
        <!-- <lifetime>30</lifetime> -->
        <lifetime>1</lifetime>
        <CashFlow name="capex" type="one-time" taxable="True" inflation="none" mult_target="False">
          <driver>
            <variable>BOP_capacity</variable>
          </driver>
          <reference_price> <!-- [-500e6, -700e6] (Hill, 2022) -->
            <fixed_value>-61.111e6</fixed_value>  <!-- Scaled for 1 year -->
            <!--<fixed_value>-600e6</fixed_value>-->  <!-- Value for 30-year lifetime -->
          </reference_price>
          <!-- <depreciate>15</depreciate> -->
        </CashFlow>
        <CashFlow name="FOM" type="repeating" period="year" taxable="True" inflation="none" mult_target="False">
          <driver>
            <variable>BOP_capacity</variable>
          </driver>
          <reference_price> <!-- [-40e6, -60e6] (Hill, 2022) -->
            <fixed_value>-50e6</fixed_value>
          </reference_price>
        </CashFlow>
        <CashFlow name="VOM" type="repeating"  taxable="True" inflation="none" mult_target="False">
          <driver>
            <activity>electricity</activity>
          </driver>
          <reference_price> <!-- [0, -2e3] (Hill, 2022) -->
            <fixed_value>-1e3</fixed_value>
          </reference_price>
        </CashFlow>
      </economics>
    </Component>

```

```
132     <Component name="HTSE">
133       <produces resource="H2" dispatch="independent">
134         <capacity resource="H2">
135           <sweep_values debug_value="6000">3000, 4000, 5000, 6000, 7000<
/sweep_values> <!-- kg/h -->
136         </capacity>
137         <consumes>electricity,heat</consumes>
138         <transfer>
139           <linear>
140             <rate resource="heat">-0.0783</rate>
141             <rate resource="electricity">-0.3269</rate>
142             <rate resource="H2">7970.4</rate>
143           </linear>
144         </transfer>
145       </produces>
146       <economics>
147         <lifetime>1</lifetime>
148         <CashFlow name="capex" type="one-time" taxable="True" inflation="none"
mult_target="False">
149           <driver>
150             <variable>HTSE_capacity</variable>
151           </driver>
152           <reference_price>
153             <fixed_value>-2690.534979</fixed_value> <!-- $/kg/h HTSE capacity -
->
154           </reference_price>
155         </CashFlow>
156         <CashFlow name="FOM" type="repeating" period="year" taxable="True"
inflation="none" mult_target="False">
157           <driver>
158             <activity>electricity</activity>
159           </driver>
160           <reference_price>
161             <fixed_value>-32_640_000.00</fixed_value> <!-- $/GW-yr -->
162           </reference_price>
163         </CashFlow>
164         <CashFlow name="VOM" type="repeating" taxable="True" inflation="none"
mult_target="False">
165           <driver>
166             <activity>H2</activity>
167           </driver>
168           <reference_price>
169             <fixed_value>-0.1398</fixed_value> <!-- $/kg/h H2 Try a different
value -->
170           </reference_price>
171         </CashFlow>
172       </economics>
173     </Component>
174
175     <!--DEMANDING COMPONENTS-->
```

```
176     <Component name="grid">
177       <demands resource="electricity" dispatch="independent">
178         <capacity>
179           <!-- This is as large as possible sink -->
180           <fixed_value>-100e3</fixed_value>
181         </capacity>
182       </demands>
183       <economics>
184         <lifetime>1</lifetime>
185         <CashFlow name="grid_sales" type="repeating" taxable="True" inflation="
    none" mult_target="False">
186           <driver>
187             <activity>electricity</activity>
188             <multiplier>-1</multiplier>
189           </driver>
190           <reference_price>
191             <ARMA variable="PRICE">Load</ARMA>
192           </reference_price>
193         </CashFlow>
194       </economics>
195     </Component>
196
197     <Component name="H2_market">
198       <demands resource="H2" dispatch="fixed">
199         <capacity>
200           <sweep_values debug_value="5000">-2500, -3500, -4500, -5500, -6500<
    /sweep_values>
201         </capacity>
202       </demands>
203       <economics>
204         <lifetime>1</lifetime>
205         <CashFlow name="H2_sales" type="repeating" taxable="True" inflation="
    none" mult_target="False">
206           <driver>
207             <activity>H2</activity>
208             <multiplier>-1</multiplier>
209           </driver>
210           <reference_price>
211             <fixed_value debug_value="4.00">4.50</fixed_value> <!-- Try a
    different value -->
212           </reference_price>
213         </CashFlow>
214       </economics>
215     </Component>
216
217     <!--STORAGE COMPONENTS-->
218     <Component name="TES">
219       <stores resource="heat" dispatch="independent">
220         <capacity resource="heat"> <!-- (500 - 345) * (boost time = 5.5 hr) /
```

```
(BOP eff = 0.4) / (TES SQRT RTE = sqrt(0.93)) -->
            <sweep_values debug_value="2.288">2.288, 3, 3.5, 4</sweep_values>
          <!-- <opt_bounds debug_value='2.288'>2.0,4.456</opt_bounds> -->
        </capacity>
        <RTE>1.0</RTE>
      </stores>
      <economics>
        <!-- <lifetime>30</lifetime> -->
        <lifetime>1</lifetime>
        <CashFlow name="capex" type="one-time" taxable="True" inflation="none" mult_target="False">
          <driver>
            <variable>TES_capacity</variable>
          </driver>
          <reference_price> <!-- [-1.929e6, -11.572e6] @ 93% RTE, 40% BOP eff, (Mikkelson, 2022) -->
            <fixed_value>-0.600e6</fixed_value>  <!-- Scaled for 1 year -->
            <!--<fixed_value>-6.75e6</fixed_value>-->  <!-- Value for 30-year lifetime -->
          </reference_price>
          <!-- <depreciate>15</depreciate> -->
        </CashFlow>
        <CashFlow name="FOM" type="repeating" period="year" taxable="True" inflation="none" mult_target="False">
          <driver>
            <variable>TES_capacity</variable>
          </driver>
          <reference_price> <!-- [-14e3, -43e3] (Hill, 2022) -->
            <fixed_value>-28.5e3</fixed_value>
          </reference_price>
        </CashFlow>
      </economics>
    </Component>

    <Component name="H2_storage">
      <stores resource="H2" dispatch="independent">
        <capacity resource="H2">
          <sweep_values debug_value="36000">30000, 35000, 40000</sweep_values>
        </capacity>
        <initial_stored>
          <fixed_value>0.2</fixed_value> <!-- Try a different value -->
        </initial_stored>
      </stores>
      <economics>
        <lifetime>1</lifetime>
        <CashFlow name="capex" type="one-time" taxable="True" inflation="none" mult_target="False">
          <driver>
            <variable>H2_storage_capacity</variable>
          </driver>
```

```
          <reference_price>
            <fixed_value>-38.00</fixed_value> <!-- $/kg Try a different value -
->
          </reference_price>
        </CashFlow>
        <CashFlow name="FOM" type="repeating" period="year" taxable="True"
inflation="none" mult_target="False">
          <driver>
            <variable>H2_storage_capacity</variable>
          </driver>
          <reference_price> <!-- [-14e3, -43e3] (Hill, 2022) -->
            <fixed_value>-9</fixed_value>
          </reference_price>
        </CashFlow>
      </economics>

    </Component>

    <!-- source of H2 in case the optimizer makes the htse smaller than H2
market it can get H2 from here but at imense cost (keeps sim going)-->
    <Component name="import_H2">
      <produces resource="H2" dispatch="independent">
        <capacity resource="H2">
          <fixed_value debug_value="6000">10000</fixed_value> <!-- kg/h -->
        </capacity>
      </produces>
      <economics>
        <lifetime>1</lifetime>
        <CashFlow name="import" type="repeating" taxable="True" inflation="
none" mult_target="False">
          <driver>
            <activity>H2</activity>
            <multiplier>-1</multiplier>
          </driver>
          <reference_price>
            <fixed_value>1e9</fixed_value> <!-- $/kg/h HTSE capacity -->
          </reference_price>
        </CashFlow>
      </economics>
    </Component>

  </Components>

  <DataGenerators>
    <ARMA name="Load" variable="PRICE" evalMode="clustered">
../arma_training/CAISO/caiso_2022_varma_clustered.pk</ARMA>
  </DataGenerators>
</HERON>

```